Mechanism of Crossover Patterning

A Thesis submitted to
Indian Institute of Science Education and Research, Pune
in partial fulfilment of the academic requirements
for the BS-MS Dual Degree Programme
by

Neel Ajay Shah

Indian Institute of Science Education and Research Pune
Dr. Homi Bhabha Road, Pashan, Pune 411008, INDIA.

Under the guidance of

Prof. Dr. Raphaël Mercier, Department of Chromosome Biology
Max Planck Institute for Plant Breeding Research, Cologne, Germany
From May 2023 to Mar 2024

Certificate

This is to certify that this dissertation entitled Mechanism of Crossover Patterning towards the partial fulfilment of the BS-MS dual degree programme at the Indian Institute of Science Education and Research, Pune, represents study/work carried out by Neel Ajay Shah at the Max Planck Institute for Plant Breeding Research under the supervision of Prof. Dr. Raphaël Mercier, Director, Department of Chromosome Biology during the academic year 2023-2024.

Raphaël Mercier

Raphael Mercier
Digitally signed by Raphael Mercier
Date: 2024.05.16 11:03:42 +02'00'

Thesis Advisory Committee:

Raphaël Mercier
Department of Chromosome Biology
Max Planck Institute for Plant Breeding Research

Mridula Nambiar
Department of Chromosome Biology
Indian Institute of Science Education and Research Pune

This thesis is dedicated to my family,
My cornerstone for patiently enduring my absence while I chased my passion

To the wonderful people I met in Cologne who turned a new city into a place I call home

Declaration

I hereby declare that the matter embodied in the report entitled Mechanism of Crossover Patterning are the results of the work carried out by me at the Indian Institute of Science Education and Research, Pune under the supervision of Prof. Dr. Raphaël Mercier, Director, Department of Chromosome Biology, Max Planck Institute of Plant Breeding Research, and the same has not been submitted elsewhere for any other degree. Wherever others contribute, every effort is made to indicate this clearly, with due reference to the literature and acknowledgement of collaborative research and discussions.

Neel Ajay Shah
20191045

16th May 2024

Table of Contents

List of Tables

List of Figures

Abstract

Crossover recombination (COs) is central to meiosis where reciprocal exchange of chromosome fragments between parental genomes occurs, shuffling chromosomes and making each offspring unique. COs are formed via homologous repair of programmed DNA double-strand breaks (DSBs) by two major pathways – the Class I pathway, catalysed by a meiotic specific group of proteins known as ZMMs, represent most COs; the minor Class II pathway forms the remaining COs, also involved in DSB repair of somatic cells. Despite DSBs occurring throughout the genome, CO placement is precisely patterned and subject to a phenomenon termed interference where COs on the same chromosome do not occur in close proximity, the mechanism of which remains elusive. To identify novel actors that regulate CO designation along chromosomes during meiosis, we adopt TurboID(TbID) based proximity labelling for meiotic cells of *Arabidopsis thaliana*. TbID tagged transgenic lines to the meiotic chromosome axis proteins REC8, ASY1/3; the transverse element of the synaptonemal complex ZYP1a/b; ZMM proteins ZIP4, HEI10 and the MutLγ resolvase MLH3 were employed as baits. Interestingly examining complementation of these transgenic lines revealed tagging *REC8* by the TbID construct results in fertility loss supposedly due to premature depletion in pericentromeric REC8, serving as valuable tool to study centromere proximal COs in the future. Current evidence suggests that the ZMM protein HEI10, which encodes a conserved RING domain containing E3 ubiquitin ligase plays a more central role in CO designation through a diffusion-mediated coarsening process. Here, we discover a RING domain mutant of AtHEI10 showing a significant decrease in fertility, highlighting the indispensable role of this domain in CO patterning plausibly through ubiquitination. Further, by mutating the Leucine 74 residue of HEI10 predicted to impede HEI10 tetramerisation based on Alfafold2 predictions, we also show that higher-order interactions of HEI10 might plausibly govern its coarsening dynamics. Taken together this study further refines our understanding of CO patterning during meiosis.

Acknowledgements

This dissertation project has been an exciting scientific pursuit. I am deeply grateful to the many individuals who made this journey fruitful, and I want to express my deep thanks to all of them.

Firstly, I would like to express my most profound appreciation to Raphaël for allowing me to work on this enigmatic project of crossover patterning, which has been a stimulating experience and also for providing me with the best available research facilities to work with at the MPI PZ. Despite a dozen other things on his plate, I find it surprising how Raphael always finds time to attend to your queries, and I'm very grateful to him for that, along with his continuous support throughout. I would also like to express my sincere gratitude to Hernán for his constant guidance and mentoring that enabled the execution of experiments planned for my thesis. I am also incredibly grateful to him for taking time out to provide periodic suggestions about experimental design to test various hypotheses. I sincerely thank our Lab manager, Alexandra Kalde, for her technical support and aid in genotyping and sample collection. I acknowledge that the results presented in my thesis are a result of collaborative research both within and beyond the group. I extend my sincere thanks to all the individuals involved in the HEI10 coarsening dynamics project, namely Hernan Lopez, Stephanie Durand, Côme Emmenecker and past lab members Juli Jing and Dipti Vernekar along with our collaborators John Weir, Raphaël Guerois and David Zwicker. I also thank my TAC supervisor, Dr. Mridula Nambiar, for her support and for introducing me to the topic of crossover interference through her Yeast Genetics course.

I was fortunate to get the opportunity to work with such wonderful lab members. I thank all of them for providing me with an excellent work environment and shout out to the vibrant, dynamic and inspiring researchers from the Department of Chromosome Biology, MPIPZ. Special thanks to Dr Sara Stolze and Anne Harzen from the Protein mass spectrometry service, Ton Timmers from the Central Microscopy (CEMIC) facility, the Greenhouse team, the IT department and Scullery at MPIPZ, which ensured the smooth execution of this project. I'm grateful to Aaron Lawson from Paul Schulze-Lefert's group for his guidance in adapting the *Nicotiana benthamiana-based* protein expression platform for HEI10's protein purification.

I want to thank the Max-Planck-Gesellschaft (MPG) and Indian Institute of Science Education Research (IISER), Pune, for making this collaborative Master's thesis

internship possible. I am deeply grateful to the Department of Science and Technology (DST), India, for their constant support in my academic journey through the SHE INSPIRE fellowship program and the Infosys Foundation for their scholarship for the academic year 2023-24. I also acknowledge Innoplexus Consulting Services' CSR support in helping me fund my travel to Germany. Last but not least, I also want to thank my family members and friends for their constant motivation, for being there for me at all times and for making this journey memorable.

Contributions

Contributor name	Contributor role
RM, HL, RG, JW, NS	Conceptualization Ideas
RM, HL, NS	Methodology
NS	Software
NS, HL	Validation
NS	Formal analysis
NS, HL, AK, SD	Investigation
HL, JJ	Resources
NS	Data Curation
NS	Writing - original draft preparation
HL, RM	Writing - review and editing
NS	Visualization
HL, RM	Supervision
RM	Project administration
RM	Funding acquisition

Contributor name
AK – Alexandra Kalde
HL – Hernán López
JJ – Juli Jing
JW – John Weir
NS- Neel Shah
RG – Raphaël Guerois
RM – Raphaël Mercier
SD – Stéphanie Durand

Chapter 1 Introduction

1.1. Background

Meiosis is a hallmark of sexual reproduction which enables the segregation of homologous chromosomes and halving the chromosome content of cells by creating unique haploid gametes which are a mosaic of parental genomes. The union of the male and female haploid gametes in a zygote then restores the offspring's ploidy back to the basic cellular diploid state. This is achieved during meiosis by carrying out a single round of DNA replication followed by two successive rounds of nuclear division realized during meiosis I and meiosis II. What makes meiosis I unique is that it involves the segregation of homologous chromosomes which allow reducing the cells ploidy by half resulting in a dyad of haploid cells. This is followed by meiosis II where sister chromatids are segregated similar to mitosis eventually resulting in the formation of four haploid gametes, which are a patchwork of parental genomes making each offspring unique.

1.2. Meiosis is a modified miotic program

The two chromosome segregation events during meiosis are dependent on a series of modifications in comparison to mitosis. First, the fidelity of the first meiotic division is reliant on crossover recombination (CO), which, in conjunction to pairing, synapsis and sister chromatid cohesion, is essential to form a physical link between homologous chromosomes in the form of bivalents, holding them together for much of meiosis. The presence of at least one CO per bivalent is a prerequisite for the correct segregation of homologs during meiosis I, without which the production of viable gametes is compromised. Second, precise regulation of sister chromatid cohesion, release, and kinetochore orientation is pivotal to maintain balanced chromosome distribution at each step of meiotic division. Lastly, the regulations of the cell cycle which ensures an strict alternation between replication of the genome and division, must be relaxed to avoid an intervening replication event between the two meiotic divisions [1]. Meiotic crossovers are necessary not only for the faithful segregation of chromosomes during the first meiotic division but also for mixing genetic material from either parent to create unique individuals. This results in genetic diversity among individuals within a population, making meiosis and, specifically, meiotic recombination as crucial genetic pathways that most likely might have contributed to the remarkable success of eukaryotes [2].

1.3. Arabidopsis thaliana as a model system to study meiosis

Meiosis arose early in the course of eukaryote evolution [3]. Recent genetic, molecular, and phylogenetic investigations have demonstrated the extensive conservation of the core meiotic machinery across taxa ranging from animals, fungi, and plants. Nonetheless, notable differences exist between species. Within flowering plants, meiosis takes place in the anther (the male organ) and the ovule (the female organ) situated within the gynoecium of the ovary. Both male and female meiosis yield haploid spores, which subsequently undergo further development via mitotic divisions and cellular differentiation into gametophytes.

Due to the relative ease of obtaining male meiocytes by observing their underlying chromosome dynamics in various flowering plants, plants have been extensively investigated using cytogenetics and genetics to elucidate the process of meiosis [4–11]. However, the emergence *of Arabidopsis thaliana* as a model species in the late 1990s enabled researchers to integrate cytological, molecular, and genetic approaches, resulting in significant progress in comprehending the meiotic program [1]. These advancements were further supported by the availability of the completely sequenced genome of *Arabidopsis thaliana* and publicly accessible collection of T-DNA insertional lines for *Arabidopsis*, which greatly facilitated the identification of several meiotic genes by genetic screens [12].

In Arabidopsis, male meiosis takes place during anther stage 6 [13], where the meiocytes are enclosed by four layers of somatic cells [14], which fall within stage 9 of flower development [13]. Every flower of *Arabidopsis* contains six anthers, each with four lobes containing around 30 meiocytes per lobe, resulting in approximately 700 meiocytes per flower. In contrast to male meiosis, female meiosis in *Arabidopsis* happens in only about 50 cells per flower, with one in each ovule. Thus, the limited number of female meiocytes and presence of somatic cells surrounding each ovule pose challenges in analysing female meiosis compared to male meiosis.

Figure 1| Schematic of reproductive structures harbouring meiocytes in *Arabidopsis* Each inflorescence contains numerous flower buds in various stages of development. Every bud is diecious and contains both the male and female floral organ namely, stamen and pistil. Male meiosis occurs in flower buds that are roughly 0.8 mm long, have a round shape, and display small petals which do not envelop the anthers where male meiosis progresses. Within each anther are four pollen sacs and the meiocytes are in the central region enveloped by the somatic cell layers of the tapetum, middle layer, endothecium, and epidermis. Female meiosis

slightly later after male meiosis in gynoecium of elongated flower buds that are roughly 1.2 mm long . Courtesy [14]

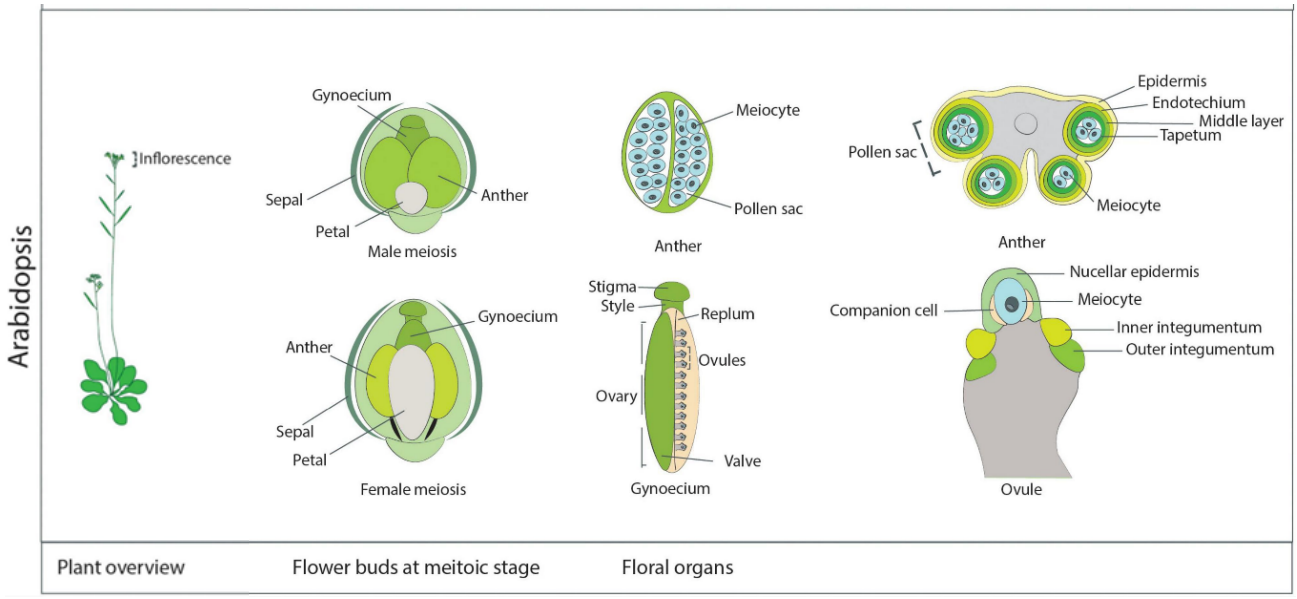

1.4. Initial Stages of Meiotic Recombination

Central to meiosis is crossover recombination (COs) where the reciprocal exchange of chromosome fragments between parental genomes occurs. COs are negatively regulated in mitotically proliferating cells during DNA repair of Double Strand Breaks (DSBs), as these could potentially risk loss of heterozygosity or cause chromosome rearrangements (especially between non-allelic repetitive sequences)[15]. To prevent crossovers, a mechanism promoting non-crossover outcomes, where only a small section of DNA is exchanged between the chromosomes, is promoted by helicases which disassemble the recombination intermediates [16]. Conversely, in meiotic cells, DSB repair as crossover is achieved through the addition of numerous meiosis-specific refinements to the DSB repair process. Meiotic recombination occurs within a highly ordered protein meshwork called the synaptonemal complex (SC), which glues together homologous chromosomes during the meiotic prophase. Chromosomes during this period of meiotic prophase which precedes meiotic divisions are characterised by the interactions among three components [10]: the chromatin of each homologous chromosome, the lateral element proteins of the SC which polymerize at the base of the sister chromatids of each homologous chromosome and the central element of the SC, which also contains the transverse elements proteins zipping together homologous chromosomes [17]. Meiotic recombination is triggered by the initiation of programmed DNA double-strand breaks (DSBs) catalyzed by the meiosis-specific transesterase Spo11 at early leptotene [18,

19]. Spo11 possesses a DNA-binding domain that is not sequence-specific and relies on the assistance of various other factors to induce DSBs [20]. Subsequently, these DSBs undergo resection by the nucleolytic activity of the MRX/MRN complex along with Com1/Sae1, generating 3'-ssDNA ends [21]. The RPA complex (RPA1/2/3) shields these single-stranded DNA strands from degradation by DNA nucleases. These RPA-bound single-stranded DNA are then recognised by the ATR kinase [22, 23]. As DNA damage-responsive kinases, ATM and ATR phosphorylate downstream effector kinases such as CHK2 (RAD53) and CHK1, respectively. During this phosphorylation cascade, BRCA1, an intermediate factor in DSB repair is also phosphorylated by ATM and ATR [24], thereby recruiting BRCA2. BRCA1 and BRCA2 facilitate the recruitment of strand invasion proteins RAD51 [25, 26] and DMC1, which bind to these ssDNA fragments initiating strand invasion [27]. Following DNA replication, three intact DNA polymers could potentially serve as templates for strand invasion in a diploid cell: the sister chromatid of the invading strand or the two non-sister chromatids of the homologous chromosomes. The meiosis-specific recombinase DMC1 and the chromosome axis components make the homologous chromatid the favoured substrate in meiosis [28]. This results in the two homologous chromosomes becoming linked by the invading DNA strand, leading to forming of a joint molecule (JM) at the joining site. The strand invasion step creates a displacement loop (D-loop) by the extension of the invading strand via DNA polymerases. Most of these intermediates are repaired through synthesis-dependent strand-annealing pathway (SDSA). Alternatively, a double Holiday junction(dHJ) can be formed through second-end capture, which can once again be removed by a complex involving DNA helicases and topoisomerase complex [29]. In both scenarios, the outcome is a non-crossover (NCO) event, where is small local patch of the intact homolog is used to repair the broken chromosome. Thus, only a small fraction of these DSBs progress to form a crossover event in the end.

1.5. Molecular portrait of DSB resolution as Crossovers

Virtually all eukaryotes, including all plants examined to date, exhibit a well conserved meiotic crossover pathway known as the ZMM pathway [32], which is responsible for approximately 85% of observed COs in *Arabidopsis*. The term ZMM originates from the initials of the proteins essential for this mechanism in yeast: ZIP (ZIP1, ZIP2, ZIP3, and ZIP4), MER3 and MSH (MSH4 and MSH5) in addition to Spo16 [30, 31]. The *Arabidopsis* equivalent of these proteins are ZYP1, SHOC1,

HEI10, ZIP4, MER3/RCK, MSH4, MSH5 and PTD [29]. The ZMM proteins create an environment that stabilises D-loops enabling formation of a double Holliday junctions (dHJs) and their subsequent resolution as COs through the activity of meiosis-specific MutLγ complex composed of MLH1-MLH3 [32]. Crossovers generated by the ZMM pathway are known as Class I crossovers, detected cytologically through the immunolocalisation of ZMM proteins MLH1, MLH3 or HEI10 in the late pachytene/diakinesis stage [33, 34]. A minor proportion of COs (roughly 15% COs in *Arabidopsis*) are produced by the Class II pathway, which operates independently of ZMMs and depend on the structure-specific nucleases like Mus81-Mms4 (part of the XPF endonuclease superfamily) crucial for DNA damage repair in somatic cells [35]. However, the resolution of dHJ intermediates by Mus81-Mms4 leads to a combination of COs and NCO products unlike the MutLγ resolvase MLH1/MLH3 heterodimer involved in Class I crossovers. These class II crossovers are negatively regulated by helicases FANCM or RECQ4 which eliminate intermediates that could potentially be utilised for MUS81-dependent crossover formation [36, 37], indicating that additional recombination pathways in plants mainly function as a backup to the class I pathway.

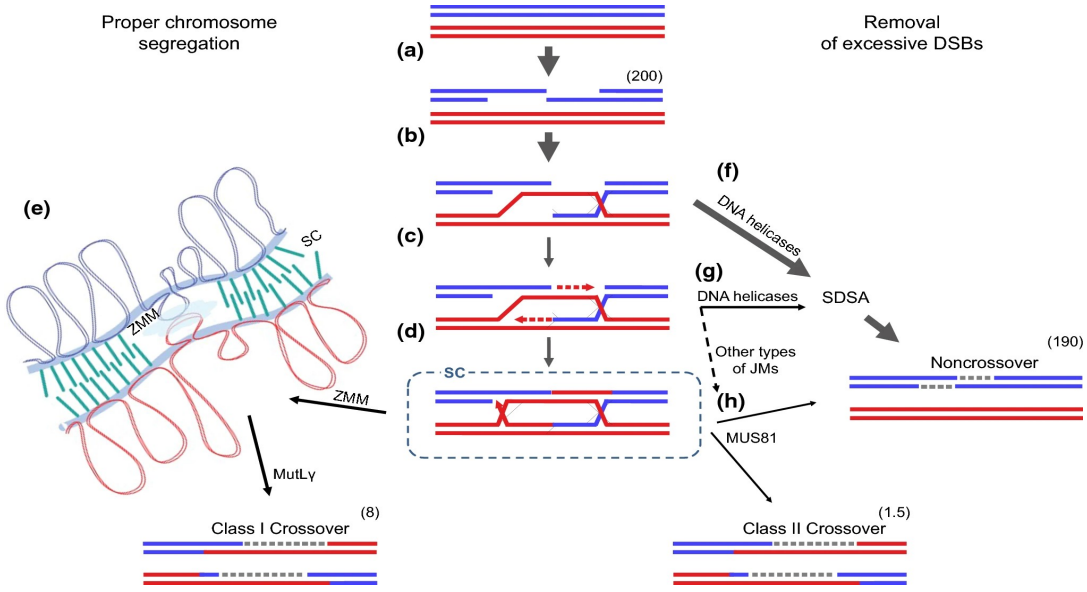

Figure 2| Model of meiotic recombination / DNA repair pathways downstream of DSB induction Meiotic recombination is initated with DSB formation and subsequent 5'→3' DNA end resection (a). Invasion of a 3' single-stranded DNA into the homologous chromatid forms a D-loop (b). This can result in DNA synthesis (dashed arrows) and subseqeuntly in second-end capture resulting in dHJ formation (c, d). dHJs, if protected by ZMM proteins, form Class I crossovers resolved by the MutLγ resolvase. This occurs in the environment of the SC, which regulates Class I crossover distribution (e). DSBs not designated as crossovers are repaired by pathways such as synthesis-dependent strand annealing (SDSA), resulting in NCOs (f, g). The few JMs (including dHJs) which have escaped being unravelled by DNA helicases (mainly RECQ4 and FANCM) (g) can eventually be resolved by MUS81-MMS4 to produce either a CO or an NCO (h). The approximate number of each of these event per generation in *Arabidopsis* during meiosis is indicated in brackets. Courtesy [38]

1.6. The ZMM pathway ensures multi-level regulation of crossover recombination

One may wonder why the Mus81 endonuclease pathway is not the dominant crossover pathway in plant meiosis. A possible explanation can be found by observing Fission yeast and several Aspergillus species, which solely depend on Mus81 for crossover recombination. These species do not possess ZMM proteins, engage in DSB-independent chromosome pairing, lack the conventional SC and crossover interference, and have higher crossover numbers per chromosome compared to ZMM-containing organisms [10, 39]. This elevated number of COs can be justified by the necessity of at least one CO per chromosome pair, a requirement that can only be met by a relatively high CO frequency due to the random placement of Class II COs. [40]. Research in *Arabidopsis* has indicated that the MUS81-dependent CO pathway avoids interhomolog polymorphisms during CO resolution. This is supported by findings on the Arabidopsis FANCM mutant, which enhances MUS81-dependent COs and leads to a significant rise in CO frequency, specifically in inbred lines, rather than hybrid plants.[36, 41]. Conversely, the ZMM pathway involving the MSH4-MSH5 heterodimers from the MutS mismatch repair protein family may be more accommodating to mismatch containing heteroduplexes [46] and thus are in a better position to cope with heterozygosity encountered during outcrossing and circumventing the costs associated with inbreeding and homozygosity[42]. The SC in plants not only plays a role in chromosome pairing but also influences the frequency and distribution of Class I COs. Mutants with impaired SC formation in *Arabidopsis* exhibit an increase in Class I COs, loss of interference, and slightly reduced fertility due to the absence of crossover assurance [43]. Therefore, the ZMM pathway, in conjunction with the SC, offers a comprehensive regulation of CO distribution at multiple levels. While the MUS81 pathway has the potential to mend DSBs, it is difficult to tune and primarily serves as an emergency brake that is typically downregulated, at least in plants[38].

Table 1| Overview of proteins involved in Meiotic prophase I During the meiotic prophase homologous chromosomes undergo pairing, synapsis and recombinaiton through a conserved molecular process to ensure accurate segregation of homolgos. The main proteins invovled in this process is indicated for different organisms namely *S. cerevisiae*, *C. elegans*, *D. melanogaster* (females), *A. thaliana*, and *M. musculus*. Courtesy [44]

Table 2| Comparison of crossover control between ZMM- and Mus81- dependent pathways Regulation of the initial stages of meiotic recombination including that conferred by ZMMs is not included. The question marks indicate potential uncharacterized factors regulating Class II COs. Courtesy [38]

	Chromosome axis		Synaptonemal complex		Double strand break formation		End Resection	Strand invasion	Non Crossover	dHJ dissolution	double Holliday junction (dHJ)	dHJ resolution
	Sister chromatid cohesion	Axial elements	Lateral elements	Central Region	DSB core complex	DSB accessory proteins						
S. pombe	Rec8	Red1 Hop1	Red1 Hop1	Zip1 Ecm11 Gmc2 SUMO	Spo11 Rec102 Rec104 Ski8	Mei4 Rec114 Mer2	Mre11 Rad50 Xrs2 Sae1 Exo1 Rpa1	Rad51 Dmc1	Mus81 Mms4 Slx1/4 Yen1 Rad1	Sgs1 Top3 Rmi1	Mer3 Msh4/5 Zip1/2/3/4 Spo16	Mlh1/3 Exo1
C. elegans	REC-8 COH-3/4	HTP-1 HTP-2 HTP-3 HIM-3	HTP-1 HTP-2 HTP-3 HIM-3	SYP-1 SYP-2 SYP-3 SYP-4 SYP-5 SYP-6	SPO-11	DSB-1 DSB-2	MRE-11 RAD-50 NBS-1 COM-1 EXO-1 RPA-1	RAD-51	MUS-81 SLX-1/4 XPF-1 LEM-3	HIM-6 TOP-3 RMH-1	MSH-4/5 ZHP-1/2/3/4 COSA-1	SLX-1/4
D. melanogaster	Solo Sunn Ord	C(2)M	C(2)M	C(3)G Corolla Corona	Mei-W68 Mei-P22	Trem	Mre11 Rad-50 Nbs	Spn-1			Rec Mei-217 /218 Vilya Narya Nenya	Mei-9 Ercc1 Mus312 Hdm
A. thaliana	SYN1 SYN3	ASY1/3/4	ASY1 ASY3 ASY4	ZYP1A ZYP1B	SPO11-1 SPO11-2 MTOPVIB	PRD1 PRD2 PRD3 DFO PHS1	MRE11 RAD50 NBS1 COM EXO1 RPA1 A/C	RAD51 DMC1	MUS81 SEND1 ERCC1/XPF	RECQ4A/B Top3α RMI1	MER3 MSH4/5 SHOC1 ZIP4 PTD HEI10	MLH1 MLH3
M. musculus	REC8 RAD21L	SYCP2 SYCP3 HORMAD1 HORMAD2	SYCP2 SYCP3	SYCP1 SYCE1 SYCE2 SYCE3 TEX12	SPO11 TOPOVIBL	MEI1 MEI4 REC114 IHO1 ANKRD31	MRE11 RAD50 NBS1 EXO1 RPA1 MEIOB	RAD51 DMC1	MUS81 GEN1	BLM Top3α RMI1	MER3 MSH4/5 HEI10 RNF212 CNTD1	MLH1/3 EXO1

Crossover pathway	Factor	Type of regulation
ZMM (Class I Crossover)	Synaptonemal complex (SC)	CO interference CO assurance Negative control of CO number [40, 45–47]
	HEI10	Dosage-dependent CO number adjustment [48]
		CO interference (SC mediated) [43, 49]
	HSBP (HCR2)	Negative control of CO number (via repressing HEI10 expression) [50]
	HCR1 (Protein phosphatase X1)	Negative control of CO number (by phosphorylation of MutS and/or MutL complexes) [51]
	HEIP1	CO number control (mechanism unknown) [52, 53]
	MSH2 complexes	CO distribution control in response to DNA polymorphisms [54–58]
Mus81-dependent (Class I Crossovers)	FIGL1 AAA-ATPase together with FLIP	Limiting Class II CO (via inhibiting strand invasion) [41, 59, 60]
	FANCM helicase complex (FANCM, MHF1, MHF2)	Limiting Class II CO (via JM dissociation) [36, 41, 59, 61, 62]
	REQ4 helicase complex (RECQ4A/B, TOP3α, and RMI1)	Limiting Class II CO (via JM dissociation) [37, 62]
	SMC 5/6 complex (SNI1)	Limiting Class II CO (by affecting DNA helicase activity) [63, 64]

1.7. Meiotic crossover patterning

Despite the seemingly random nature of crossing-over, which can potentially happen anywhere along the chromosomes, the placement of crossovers follows intricate patterning. There are three distinct types of crossover patterning events that have been identified– 1. Interference refers to the phenomenon where crossovers on the same chromosome are not located close to one another [65] 2. Assurance explains the occurrence of at least one crossover per chromosome pair [66] 3. Suppression dictates that crossovers do not occur in centromeric and telomeric regions [67]. The mechanisms underlying crossover patterning remain largely elusive. This dissertation aims to contribute to the broader comprehension of crossover patterning events, particularly interference.

1.8. Interference

Crossover interference was first noted by Sturtevant during the construction of the first linkage map in *Drosophila melanogaster* [68]. Sturtevant observed that double

crossovers between adjacent intervals were much less frequent than expected by random chance, later shown by him to be an intra-chromosomal process [65]. The potential for CO interference operating at the chromatid level was also explored (Figure 3), i.e., when there are two crossovers on the same chromosome arm, is there an influence of the chromatids involved in one on those used in the other? Investigations in Drosophila indicated that the first crossover did not impact the chromatids involved in the second one, suggesting an absence of chromatid interference [69]. Similar findings were observed in budding and fission yeast [70, 71], although not in *Neurospora crassa* [72]. However, the prevailing view in most studies has been the absence of chromatid interference [73].

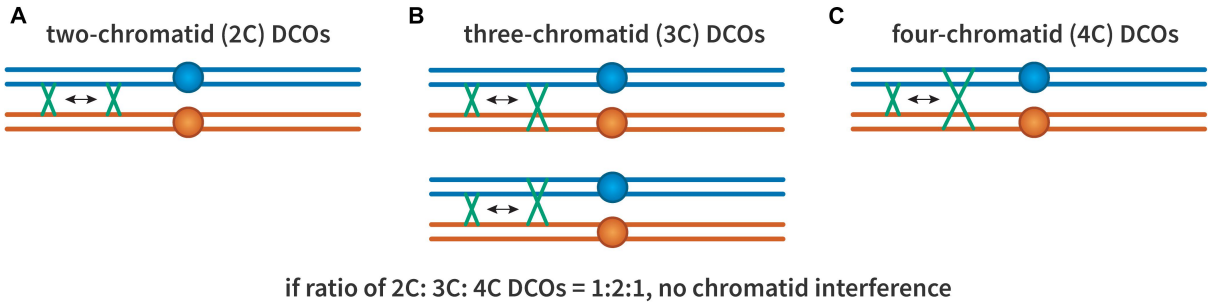

Figure 3| Chromatid interference Each panel depicts a double crossover (DCO) on a single bivalent, with each line symbolising a chromatid. The initial crossover (leftmost) is consistent across all instances, occurring between the two inner chromatids. (A) 2-Chromatid (DCO). (B) Possible configurations of a 3-chromatid DCO. (C) 4-Chromatid DCO.

The main meiotic crossover pathway in most organisms, the Class I pathway, generates COs that are interference sensitive while the Class II pathway yields interference insensitive CO [29]. The coexistence of both interfering and non-interfering COs confounds analyses to decipher the biological basis of crossover interference as anything that alters the proportion of Class I to Class II COs changes genetic readouts of crossover interference even if modification are absent in the underlying mechanisms of interference. Instances of this phenomenon are observed in hyper-recombinant mutants with elevated Class II COs [41]. Here, the quantity of Class I COs remains relatively constant, indicating interference is normal from a mechanistic perspective, but due to substantial Class II COs, interference is not detectable genetically. There exist two methods for characterising and quantifying crossover interference. The first method involves observing greater and more consistent distance between neighbouring COs than expected. This is quantified by plotting the distribution of inter-crossover distances, which can be fit to a gamma distribution with the shape parameter v, giving us a measure of strength of

interference [74]. The second method relies on quantifying the lack of adjacent Double Crossovers(DCOs) by calculating the Coefficient of Coincidence (CoC), a ratio of observed by expected DCOs for a given length interval. Interference strength here is measured as the length interval for which the CoC value reaches 0.5 [75]. It should be noted that the metric for measuring interference is um of axis/SC, as opposed to Mb of DNA, indicating that the interference signal spreads across the chromosome axes and/or the synaptonemal complex[76].

1.9. Interference models

Several models have been put forth to explain crossover interference since its discovery, with the current focus of debate being on two main models: the beam film model and the coarsening model. In physical systems, when there is a change in mechanical stress at a specific location, it redistributes from that point. The beam-film model [77] suggests that chromosomes experience mechanical stress, with precursor elements (DSBs) on their surfaces. When one of these breaks matures to designate a CO, this relieves the tensile stress that spreads outward from the designated event, preventing other precursors from reaching the necessary stress level for CO designation nearby, thereby causing interference. In line with this model, the enzyme topoisomerase II (Topo2), which can unwind or overwind DNA molecules, has been found to play a role in regulating CO interference [75].
The coarsening model, an alternative conceptual framework, presents a different viewpoint, suggesting interference is not caused by the transmission of a suppression signal. Instead, it proposes that interference occurs due to the accumulation of a pro-crossover factor at prospective CO sites at the expense of its neighbours, thereby establishing interference. This model was initially formulated and validated based on cytological evidence from Arabidopsis [53] with a similar model being independently devised by a separate research group using data obtained from C. elegans [81]. This model is based on the pro-crossover ZMM protein HEI10 (ZHP-3/4 in C.elegans) diffusing along the SC and a subsequent coarsening process governed by the Ostwald ripening leading to well-spaced CO-promoting HEI10 foci. HEI10 forms numerous small foci (Figure 4a) as chromosome synapses and is localized to the central region of the SC (Mercier et al, unpublished). With the progression of meiosis, less numerous but larger foci form (Figure 4b) based on a coarsening process where bigger foci tend to capture more material than smaller ones. As larger aggregates siphon off nearby HEI10, these foci tend to form

at a distance, resulting in interference. These large HEI10 foci then attract factors that support CO formation, such as MLH1 in plants and mammals or COSA-1 in C. elegans (Figure 4c). Recombination intermediates that do not have HEI10/MLH1 co-foci mature into non-COs by factors that inhibit CO formation, like Sgs1(atRECQ4)-Top3-Rmi, and occasionally as class II COs. The characteristics of the SC resembling a crystalline liquid may play a role in these dynamics of HEI10 [40, 82]. Despite the strength of the coarsening model in providing a logic to emergent phenomena of crossover interference, many unanswered questions remain which demands further testing and refining, some of which this project aims to address.

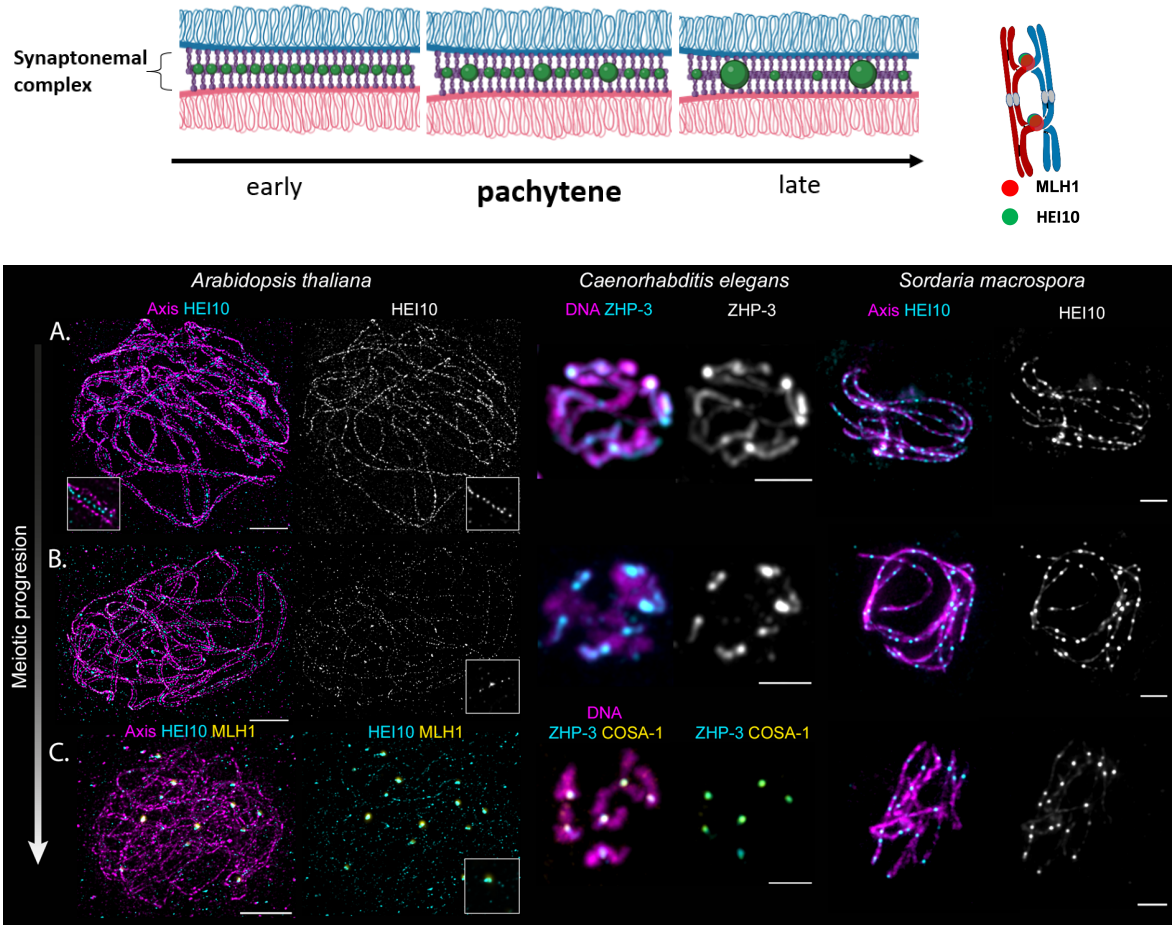

Figure 4| The coarsening model (Above) Schematic of crossover distribution along the SC as illustrated by the coarsening model. As meiosis advances, HEI10 distribution becomes more coarse, with larger foci increasing in size at the cost of smaller foci, leading to the emergence of well-spaced CO-promoting HEI10 foci reflecting interference. (Below)(A) Dymanics of HEI10 homologs based on cytology as seen *in Arabidopsis thaliana*, *Caenorhabditis elegans* and *Sordaria macrospora* Initially, HEI10 is observed as numerous small foci on chromosomes, as by shown by STED imaging in Arabidopsis with REC8 marker between axes, or as a continuous signal using confocal microscopy in *C. elegans* and wide field microscopy in *Sordaria* with Spo76/Pds5-Td Tomato marker on axes (B) During meiosis progression, some HEI10 foci increase in size with others decrease (C) Towards the conclusion of meiotic prophase, a few large HEI10 foci persists, indicating COs sites and these foci co-localize with MLH1 in Arabidopsis and COSA-1 in *C.elegans.* Scale bars 2um. Cytology images courtesy [78]

1.10. Scope of study

This project aims to further explore the mechanism of crossover patterning and test & refine our understanding of coarsening model in *Arabidosis thaliana* by discovery of novel actors regulating this process and identifying genetic backgrounds in which this process is perturbed.

AIM1: Identify the interacting partners of proteins involved in crossover designation using proximity labeling. Proximity labeling allows the direct identification of protein-protein interactions in vivo. Transgenic lines with meiotic bait proteins tagged to the proximity labelling construct will be generated and proximity labeling experiments will be performed to identify proteins involved in regulating crossover designation along chromosomes.

AIM2: Identifying novel mutants affected in crossover patterning. A collection of CRISPR-Cas9 mutants of the pro-crossover ZMM protein HEI10 will be generated to functionally characterize the role of its different domains in meiotic recombination. Based on Alphafold2 structure predictions, candidate mutations killing the predicted tetramerization of HEI10 and E3 ligase activity of HEI10 have been identified. The corresponding mutant lines will be cloned and subsequently analyzed for crossover formation using cytological techniques. Mutants with elevated or decreased crossover numbers will be further analyzed to decipher the crossover patterning process.

Chapter 2 Materials and Methods

Plant Materials and Growth Conditions. Wild type Col-0 and Ler−1 are 186AV1B4 and 213AV1B1 from the Versailles stock centre (http://publiclines.versailles.inra.fr/). The following *Arabidopsis* lines were used for proximity labelling: *zip4-2* (N568052)*, hei10-2* (N514624), *rec8-3* (N836037), *asy3-1* (N643676), *mlh3-3 (*N619674), *asy1-4* (N546272), and *zyp1ab-1* (8.7.2V1T3). HEI10 alleles for complementation were transformed in *hei10-1* (EQO124). To test dependence of ZMMs for HEI10 loading in absence of the synaptonemal complex lines used were *zyp1ab-1* (8.7.2V1T3), *zip4-2* (N568052), *mer3-1* (N545941), *msh4-1* (N636296). *A. thaliana* plants were grown in the greenhouses (16-h day/8-h night, 22 °C) or Polyklima growth chambers (16-h day, 21.5 °C, 328 280 µM; 8-h night, 18 °C: 60% humidity). Genotyping of the mutants was carried out by PCR amplification of plant genomic DNA [56].

Plant genomic DNA isolation. Plant samples were collected, frozen with liquid nitrogen and subsequently ground. 300 µl DNA extraction buffer (200 mM TRIS, 250 mM NaCl, 25 mM EDTA, 25 mM 10%SDS) was added to the ground leaves. This mix was centrifuged for 10min at 4700 rpm, and 250µl of the supernatant was transferred in fresh tubes before containing 200 µl of isopropanol. This was centrifuged for 5 minutes at 4700 rpm, and the supernatant was decanted, and pelleted DNA was allowed to dry. The DNA was resuspended in 200 µl of DNase-free water and stored at 4ºC

Agrobacterium transformation. Transformation into *Arabidopsis* plants was carried out by floral dipping[79]. Transformation of female gametes was achieved by immersing developing Arabidopsis inflorescences briefly into a 5% sucrose solution containing 0.05% (vol/vol) Silwet L-77 and resuspended *Agrobacterium* cells carrying the desired construct. Treated plants were allowed to set seed and subsequently screened for transformants using the appropriate selection marker.

CRISPR cas9 Mutagenesis. Plasmid constructs were designed as described by [80] using the Golden Gate cloning system [81]. Guide RNAs targeting *HEI10* (AT1G53490) were designed using and CHOPCHOP (https://chopchop.cbu.uib.no/) and CRISPR-P 2.0 (http://crispr.hzau.edu.cn/CRISPR2/). To increase the efficiency of gene mutagenesis, four single guide RNAs (sgRNAs) were introduced simultaneously. Single guide RNAs (sgRNAs) were developed by PCR by combining

the crRNA and the trans-activating crRNA (tracrRNA) using the pICH86966 plasmid as a template. Individual sgRNA were placed downstream of the Arabidopsis U6 promoter in the Level 1 acceptors pICH47751, pICH47761, pICH47772, and pICH47781 plasmids. The Level 1 constructs pAGM51323-AthRps5a:Cas9 (Zcas9i):nos ter, pICH50927-linker for 4 sgRNA, pICSL11015-FAST-Red, pICH47751-AtU6pro: sgRNA-1, pICH47761- AtU6pro: sgRNA-2, pICH47772-AtU6pro: sgRNA-3, and pICH47781- AtU6pro: sgRNA-4 were assembled into the binary Level 2 plasmid pAGM4723. The corresponding constructs were introduced into Agrobacterium strain GV3101 and used for Agrobacterium-mediated transformation. Transgenic plants (T1) were selected based on the seed coat RFP fluorescence marker. The selected T1 plants were screened for *hei10* deletions by PCR. Subsequently, T2 seeds devoid of fluorescence were chosen as cas9-free and again genotyped for deletion at the *hei10* locus. Deletion at the *HEI10* locus was confirmed by PCR Sanger sequencing.

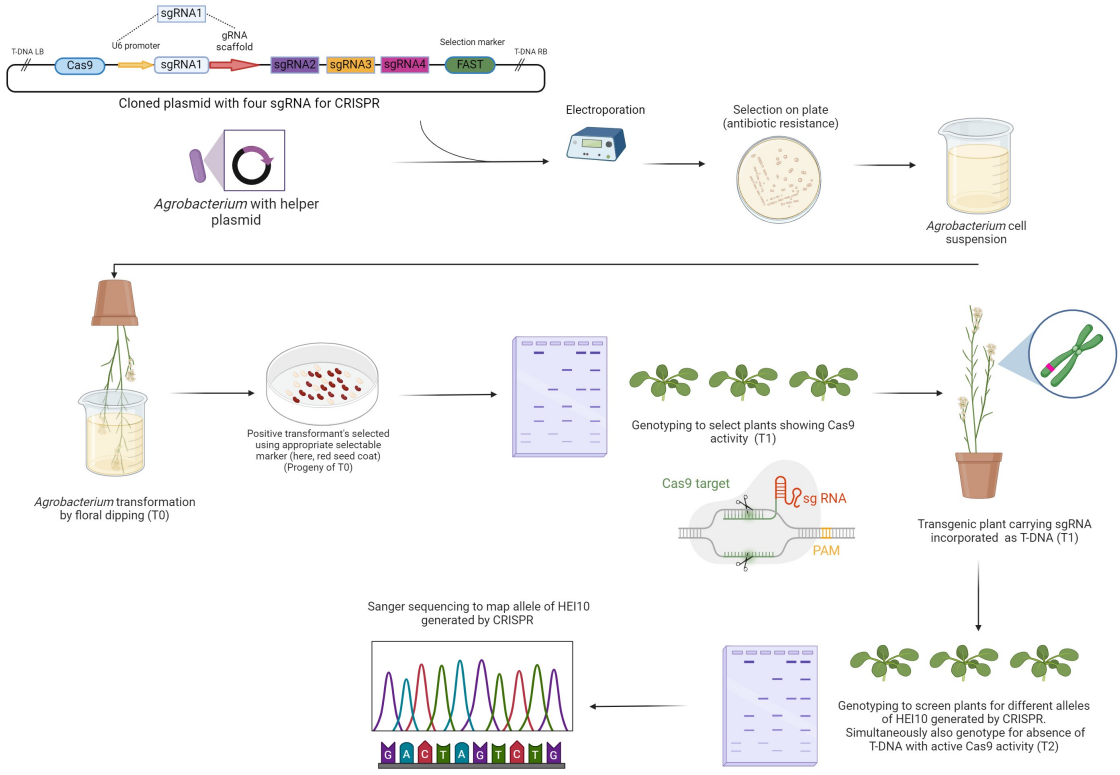

Figure 5| Workflow to screen for HEI10 alleles by CRISPR cas9 mutagenesis The level 2 binary vector with Cas9 and the four sgRNA driven by the Arabidopsis U6 promoter assembled using Goldengate cloning was transformed into Col-0 plants. After selecting positive transformants, T1 plants were screened for Cas9 activity based on *hei10* deletions detected by PCR. Subsequently, T2 seeds devoid of fluorescence were chosen as cas9-free and genotyped again at the *hei10* locus for deletions, which were confirmed by PCR Sanger sequencing.

Complementation. Plasmid constructs were designed as described by [82]. A genomic DNA fragment including the putative *HEI10* promoter was PCR-amplified with CloneAmp HiFi (TakaRa) from isolated genomic DNA of *Arabidopsis thaliana* and cloned into pGGA000 (Addgene # 48856) using NEBuilder HiFi DNA Assembly (New England Biolabs). The *HEI10* coding region was amplified in two fragments using *HEI10* cDNA as a template to synonymously mutate a *Bsa*I site. Both PCR fragments were seamlessly integrated into pGGC000 (Addgene # 48858). For mutating the RING domain of *HEI10 and* Alfafold2 predicted tetramerisation of *HEI10, the coding region was amplified using a similar approach now using domesticated HEI10 cDNA cloned in the previous step as a* template. The DNA sequence downstream of the stop codon was amplified with *HEI10* terminator primers and cloned into pGGE000(Addgene #48860). The final complementing construct was assembled using GoldenGate cloning (BsaI) by combining the promoter, genomic and terminator modules with pGGB003 (Addgene # 48821), pGGD002 (Addgene # 48834), Plant selection cassette FAST RED cassette (Addgene # 136979
136979), with pAGM4723GG (Addgene #136960) as a binary vector. The corresponding construct was introduced into *Agrobacterium tumefaciens* strain GV3101 and used for Agrobacterium-mediated transformation in *hei10-1 plants*. Transgenic plants were tested for the presence of the transgene selected based on the seed coat RFP fluorescence marker and subsequently genotyped to be homozygous for the *hei10-1* allele.

Constructs for TbID-based Proximity labelling. Plasmid construction was carried out by first PCR amplifying the putative promoter, coding sequence and terminator of the bait protein of interest into pGGA000, pGGC000 and pGGE000 Greengate modules, respectively[82]. The TbID tagged bait construct was assembled using GoldenGate cloning (BsaI) by combining the promoter, genomic and terminator modules of the bait proteins with plasmids pGGB003 (Addgene # 48821), TbID-Venus cloned in the D module (Addgene # 48859) using Plasmid Addgene #127353 as template, Plant selection cassette FAST RED (Addgene # 136979136979), with pAGM4723GG (Addgene #136960) as binary vector. In the case of internal tagging of our bait by the proximity labelling construct, the coding sequence of the bait protein was PCR amplified in two fragments and introduced into pGGB000 (Addgene # 48857) and

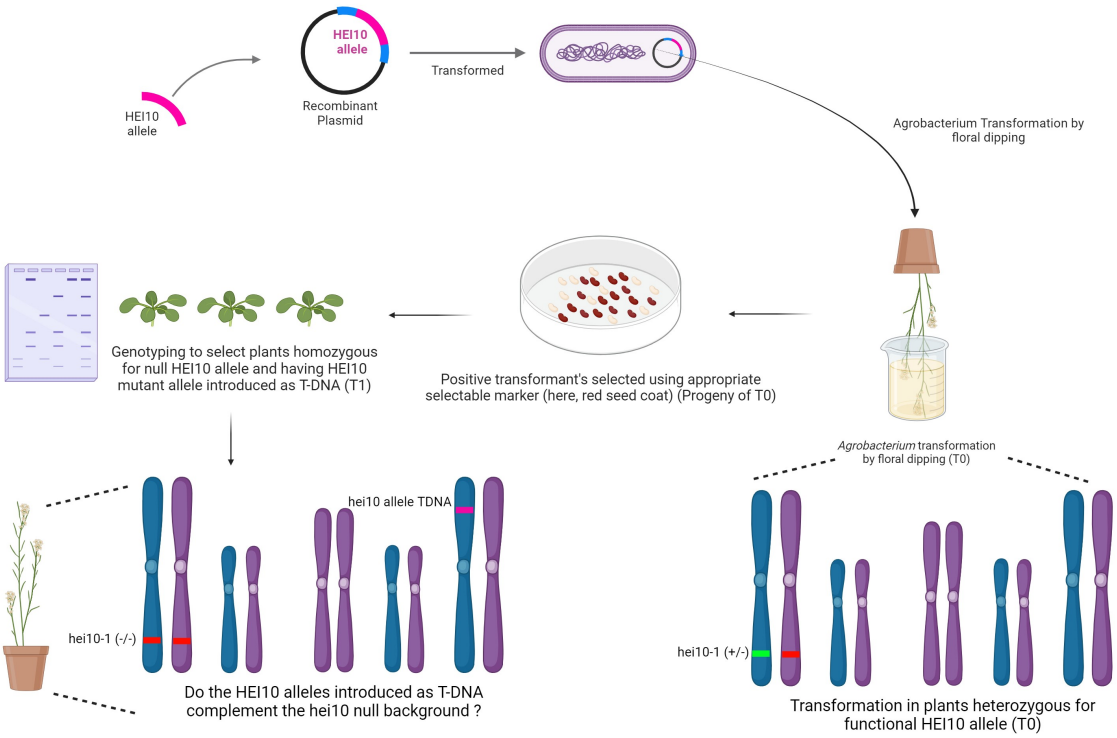

Figure 6| Overview of the methodology adopted to test complementation of HEI10 alleles **The various alleles** for HEI10 assembled using Goldengate cloning transformed into *hei-1* heterozygous for a functional *HEI10* allele. After selecting positive transformants, the plants were genotyped to select for *hei-1* in homozygous condition and to probe if the HEI10 allele introduced as T-DNA complements the HEI10 null background.

PGGD000 (Addgene # 48859) with the proximity labelling construct in the C module for assembly by Gateway cloning. However, now, for the final assembly, the TbID-Venus tag was cloned into the C module (Addgene # 48858). The corresponding construct was introduced into *Agrobacterium tumefaciens* strain GV3101 and used for Agrobacterium-mediated transformation in respective mutant backgrounds of the bait protein. Transgenic plants were selected for the presence of the transgene using the appropriate selection marker and genotyped to select heterozygous plants for the mutant background (T1). In the next generation, plants homozygous for the mutant background and Tb-tagged bait protein introduced as T-DNA were selected (T2). For selecting the T-DNA in homozygous conditions, segregation of the selection marker associated with the T-DNA in progeny of the T2 plants was assessed.

Figure 7| Generation of Transgenic plants with TbID tagged bait The level 2 binary vector with the bait protein tagged with the TbID construct (shown here as C-tag for representation) was transformed into plants heterozygous for the mutant background of the bait protein. After selecting positive transformants, T1 plants were genotyped to heterozygous for the mutant background. The progeny of the T1 plants now segregates for both the

transgene introduced as T-DNA and the mutant background null allele. T2 seed fluorescent seeds, positive for the T-DNA, are sown and subsequently genotyped to be homozygous for both the mutant background and the transgene introduced as T-DNA.

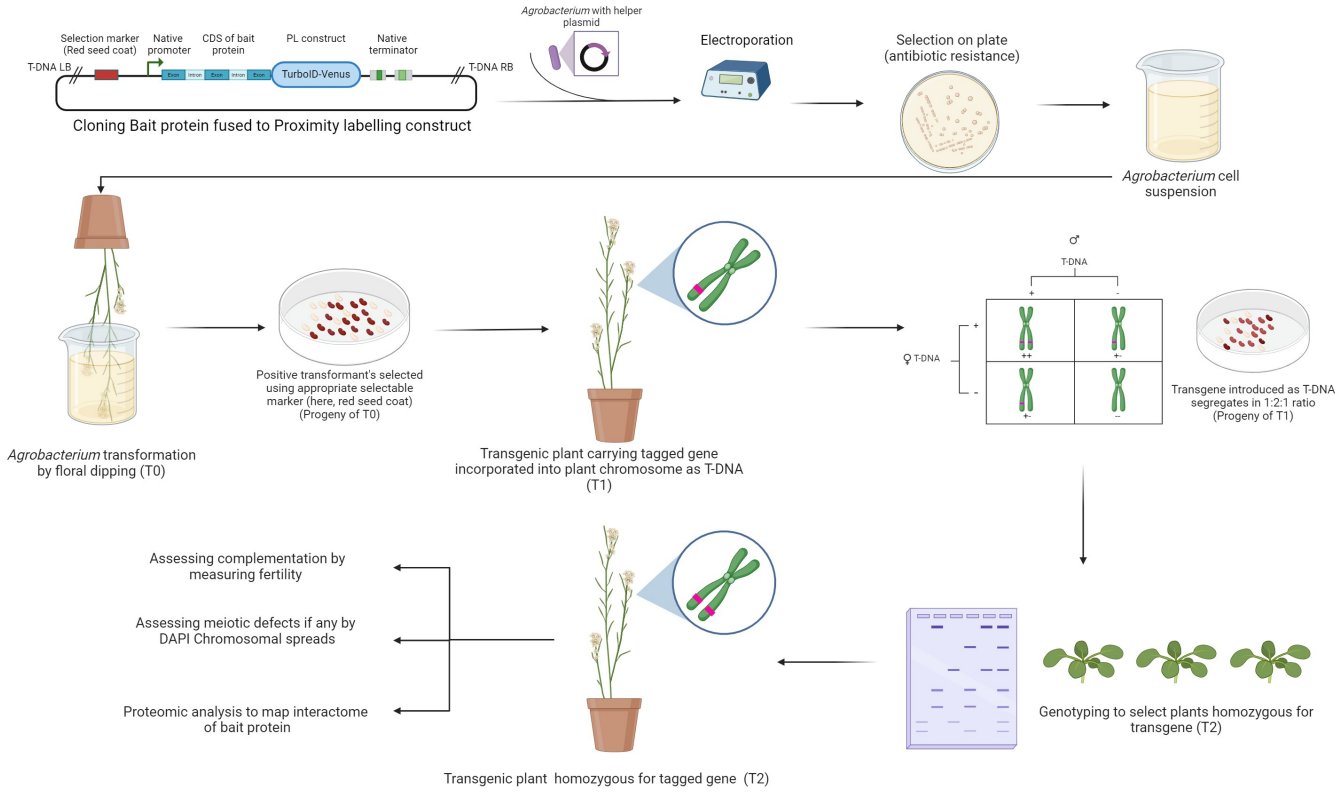

Live cell imaging of meiocytes. The methodology to observe male meiocytes using live cell imaging was adapted from [14]. Freshly harvested *A. thaliana* inflorescences with an approximate diameter of 0.4-0.6 mm were chosen, and the upper sepal was removed to facilitate observation of the undamaged anther. This dissected flower bud along with the pedicel was mounted in Arabidopsis Apex Culture Medium (ACM) consisting of half-strength Murashige and Skoog (MS) salts, 1% sucrose, and 0.8% agarose with pH 5.8 and supplements diluted to 1X from 1000X stock consisting of Myoinositol (10%), nicotinic acid (0.1%), pyridoxine hydrochloride (0.1%), thiamine hydrochloride (0.1%), and glycine (0.2%) dissolved in H2O. The embedded flower bud was stabilised with a drop of agarose, and imaging was conducted using an up-right laser scanning confocal microscope (Leica STELLARIS 8 Confocal Microscope) using the 25X water immersion objective after the flower bud was covered with a layer of water. Venus was excited at λ 515 nm and detected at λ in the 520 to 560 nm range. Autofluorescence from chloroplasts at λ between 680–750 nm was used to locate the flower buds.

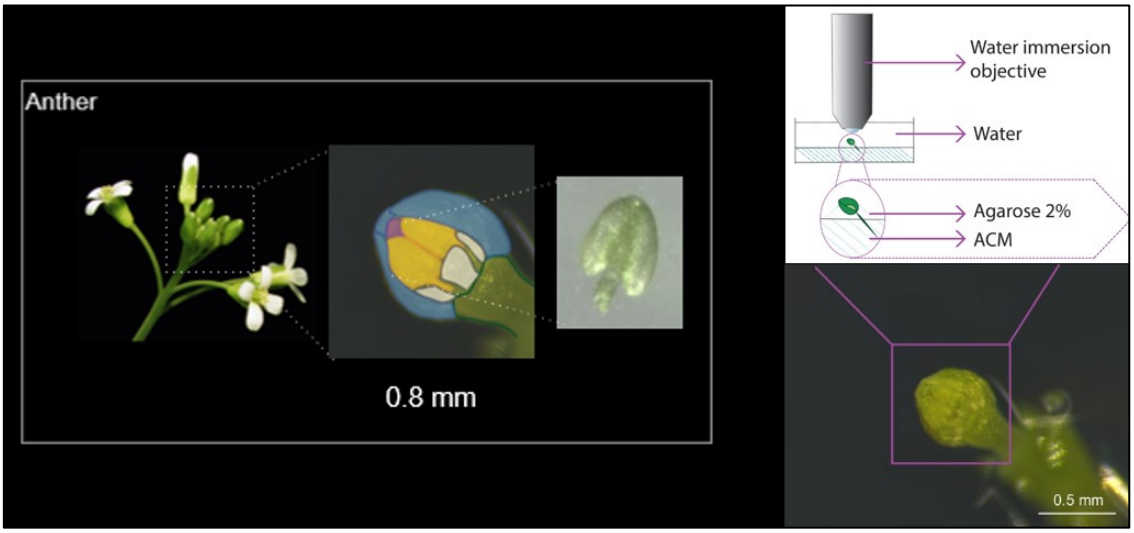

Figure 8| Live cell imaging of meiocytes in *A.thaliana*. Freshly harvested inflorescences were dissected for flower buds in the 0.5-0.8 mm size range. The upper sepal was removed to expose the anthers. This isolated flower bud is embedded on a Petri dish containing ACM medium and subsequently covered with a drop of 2% agarose and submerged in sterile water. The sample is then viewed using a water objective by bringing the lens in contact with the water

Meiotic Chromosome spreads. Meiotic chromosome spreads were carried out as described in [83]. Inflorescences were harvested in fixative with 3:1 volume of ethanol to acetic acid, and the fixative was changed twice. For preparing slides, the inflorescences were washed twice with water, followed by a wash with citrate buffer (10 m trisodium-citrate with pH 4.5 adjusted with HCl). They were digested for 2 hours at 37ºC in a humidified chamber with a digestion mix [pectolyase Y-23 (0.3% w/v), Driselase (0.3% w/v), cellulase (0.3% w/v) and sodium azide (0.1%) in 10 mM citrate buffer]. Approximately five 0.5mm washed buds were transferred to a slide with a drop of water and dilacerated with needles to create a suspension of cells. 10ul of 60% acetic acid was added to the slide and immediately transferred to a heating block at 45ºC for 1 min with the cell suspension stirred with a needle. After a minute, 10 ul of 60% acetic acid was added and stirred. The cell suspension was surrounded by fresh 3:1 fixative and flushed. The slides were left to dry and stained with a drop of DAPI (2 ug/ml) in Citrifluor AF1 (Agar Scientific). The slides were then observed using a Zeiss Axio Imager Z2 microscope, and images were acquired using Plan-Apochromat 100X/1.40 oil M27 objective. DAPI was excited at λ 335-385 nm and detected at λ in the 420 to 470 nm range.

Alexander staining. Alexander staining was performed to check for pollen viability as described in [84]. Flower buds were collected and fixed in a 6:3:1 solution of alcohol:chloroform: acetic acid for 2 hours. The buds were then placed on a slide,

and excess fixative was dabbed dry using absorbent paper, followed by dissection to release the anthers. 2-4 drops of staining solution (10 ml of 95% ethanol, 1 ml of 1% Malachite green solution prepared in 95% ethanol, 25ml of glycerol, 5 ml of 1% Acid Fuschia,0.5ml of 1% Orange G, 4ml of Glacial acetic acid was mixed and made up to a volume to 100ml adding distilled water) is added to the dissected anthers. Heat the slide over a flame burner under a fume hood until the stain nears a boil. Place a slip over the sample and seal it with nail polish. The slides were subsequently observed using a Zeiss Axio Imager Z2 microscope.

Fertility analysis. The fertility of a given line was quantified by counting the number of seeds per silique. For this, ripe siliques were harvested in 70% ethanol and scanned on a scanner by gently pressing them with a glass plate. The scanned siliques were then assessed for a number of seeds quantified using the event counter tool on Zen Blue software.

Biotin treatment of buds for TbID-based proximity labelling. Freshly cut inflorescences, along with their stem, were immersed in 0.5mM biotin (Sigma) solution overnight. After overnight biotin supplementation, roughly 300 inflorescences were fine-dissected, with the selection criteria set to a maximum size threshold of 0.5mm to capture meiosis. Post-dissection buds were frozen in liquid nitrogen and stored at -80ºC until further use.

Western blotting. Biotin-treated buds were ground using a Retsch mill in 2ml Eppendorf's using a metallic bead. 100ul of 1X RIPA lysis buffer (Merck) [10X stock solution diluted with sterile water along with Protease Inhibitor Cocktail (Merck P9599)]. The samples are spun down at 16,000 x g for 20 mins at 4ºC after incubating for 30 mins on ice. The supernatant was transferred to a fresh tube, and protein concentration was determined. An aliquot for long-term storage at -20ºC was taken. To 20ug of sample and an equal volume of 2x Laemmli sample buffer was added, and the lysate in the sample buffer was boiled for 5 mins at 95ºC followed by centrifugation at 16,000 x g for 1 min. 20ul of the sample was then loaded onto a 10 % SDS-PAGE gel for separation of proteins, followed by transfer onto a polyvinylidene difluoride membrane (Immobilon-P) for blotting. Antibodies used for blotting: HRP-Conjugated Streptavidin (1:5,000, ThermoScientifcRabbit™, N100), Rabbit mAb to Biotin (1:5,000, Abcam, AB234284), Rabbit mAb to Histone H3

(1:5,000, Abcam, AB1791) and Goat Anti-Rabbit IgG H&L(HRP) (1:4,000, Abcam, AB6721).

LC-MS analysis of Biotinylated protein by TbID tagged bait. The biotin-treated buds were ground on a Mixer Mill to obtain a fine powder to which 500ul of hot SDT buffer (100mM Tris pH7.5, 4% SDS, 0.1M DTT) was added and vortexed. The samples were then incubated for 5 mins at 95ºC followed by sonication and spinning down for 5 mins at 10,000 x g. The supernatant is then transferred to a fresh tube and centrifuged again to ensure no debris is retained. The concentration of the supernatant is determined, followed by Biotin depletion by MeOH: CHCl3. For this, after adjusting the concentration of the crude lysate to 1 ug/ul, 500ul of crude lysate is mixed with 666ul of methanol, 166ul of chloroform and 300ul ultrapure water, vortexed well and spun down for 10 mins at 4,000 rpm to separate the phases. The upper and lower phases are removed carefully only to retain the white layer in between containing precipitated proteins. This pellet is washed with 600ul of methanol and sonicated until no large fragment remains. Then, it is spun down to remove the supernatant. The protein pellet is resuspended in 125ul SDT lysis buffer, vortexed and sonicated for 10mins. The samples are then incubated for 30 minutes at 25ºC on a shaking incubator set to 1000rpm. For affinity pulldown of biotinylated proteins from the now biotin-depleted protein samples, incubate the sample dissolved in binding buffer (0.1 M phosphate, 0.15 M NaCl, 0.5% SDS, pH 7.2) with equilibrated Dynabeads Myone Streptavidin C1 (Thermo Scientific # 65601). Incubate the sample and beads at 22ºC overnight with gentle inverting for affinity pulldown of biotinylated proteins. After pulldown, spin the sample to collect the beat and remove the supernatant. Wash the beads with buffer 1 (0.1M phosphate, 0.15M NaCl, 2% SDS, pH 7.2). Centrifuge, discard the supernatant, and wash the beads thrice with wash buffer 2 (0.1 M phosphate, 0.15M NaCl). Centrifuge ,to remove the supernatant, and the beads are handed over to the Protein Mass-Spectrometry facility for an on-bead digest of proteins and subsequent Liquid chromatograph MS analysis.

Chapter 3 Results and Discussion

3.1. TurboID-based proteomic profiling of meiocytes in Arabidopsis thaliana to decipher the protein network that establishes crossover distribution along chromosomes during meiosis

Proteomic analysis in plants focused on unravelling the composition and control of proteins participating in meiotic crossover patterning has traditionally faced limitations due to the paucity of meiotic cells contained within plant floral organs. Previous approaches utilising affinity purification-based mass spectrometry have often resulted in many false positives, as interacting partners are only detected after cell lysis. Moreover, these methods were unable to capture interactions that were weak, short-lived, or confined to specific spatial and temporal conditions. The precise and thorough characterisation of these dynamic interactions are essential in proteomic research for annotating protein roles and examining the underlying biological process. Recent advancements in proximity labelling (PL) methodologies such as BioID and APEX have provided the necessary sensitivity and specificity to map protein complexes and proteomes at a cell type-specific level. These techniques involve the use of an enzyme which is tagged to a bait protein of interest, which in the presence of biotin or biotin-containing substrates, will biotinylate interacting proteins that are in close vicinity to the bait in a covalent fashion, enabling their isolation from the total protein lysate using streptavidin-conjugated beads. This allows for exploring local protein environments, including those of rare proteins or specific cell types. These proximity labelling enzymes are mainly engineered peroxidases or ligases. In Biotin ligase-based proximity labelling, in the presence of exogenous biotin, the engineered biotin ligase catalyses the conversion of biotin into a transient, readily dispersible, active intermediate, which is then conjugated to the ε-amino group of exposed lysine residues on nearby proteins in a process similar to Ubiquitination.

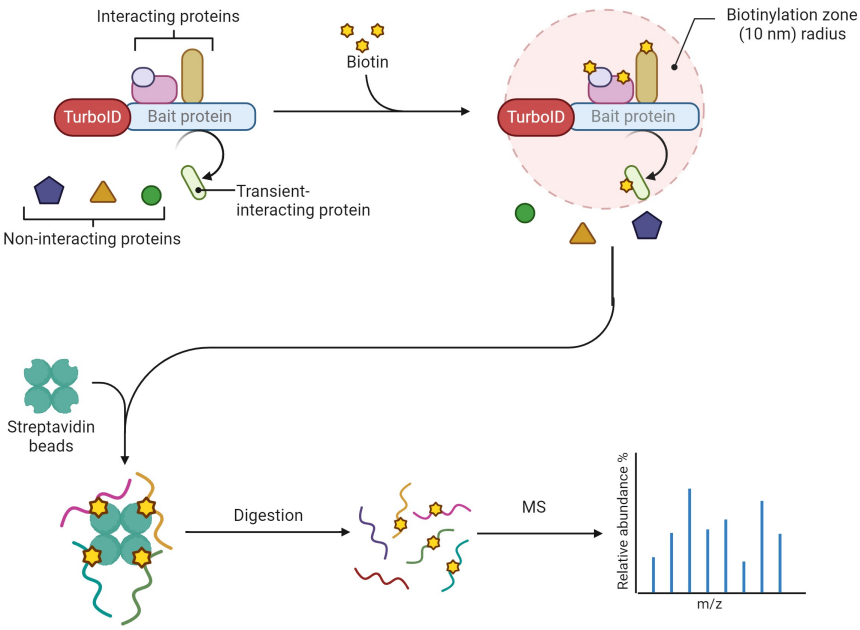

Figure 9| Principle of TurboID-based proximity labelling. The proximity labelling enzyme fused to the bait protein in the presence of biotin and ATP forms a reactive intermediate, biotinyl-5'-AMP, which biotinylates proteins within a vicinity of 10 nm (Coloured Beige). Biotinylated proteins are pulled down using streptavidin beads, followed by on-bead digestion and subsequent mass spectrometric analysis.

For achieving this, several promiscuous variants of the biotin ligase BirA have been engineered - BioID, miniTurboID and TurboID, which are derivatives of E. coli BirA; BioID2, microID2, and ultraID obtained, which are derivatives of *Aquifex aeolicus* BirA; and BASU derived from *Bacillus subtilis* [85]. All these variants share a common feature: increased dissociation rate of the active biotin intermediate (biotinyl-5'-AMP). Table 2 summarises the labelling times and working temperatures for each variant. As seen from the table, the biotin ligase, namely TurboID, boasts the highest activity of all biotin ligases and the broadest working temperature range compatible with *Arabidopsis* growth conditions. Due to its fast-labelling kinetics, it is the ideal candidate for the study of spatial and temporal dynamics, and in this study, we have utilised this construct to be fused alongside our bait proteins to map the interactome of various meiotic proteins crucial for crossover patterning. However, a limitation of TurboID to note is that its high activity also results in higher background labelling utilising endogenous biotin reserves. Further, this also results in high self-biotinylation of the TurboID fused bait, potentially impeding the bait function if the biotin-modified lysine residues on its surface are essential for its functionality.

Table 3| Comparison of various biotin ligases used for Proximity labelling – Mass spectrometry application. Courtesy [85]

Enzyme Name	Labeling time	Enzyme Name	Labeling time
BioID	18-24h, Optimum temperature 37°C	**UltraID**	≥10 min (Not tested in plants)
TurboID	≥10 min, 30-37°C temperature optimum works well at 20-25 °C	**microID2**	3h labelling time (Not tested in plants)
MiniTurboID	≥10 min, 30°C temperature optimum works well at 20-25 °C	**AirID**	3-8 h, Active in a range of 16-37 °C (Not tested in plants)
BioID2	16-24h, 50°C temperature optimum, works well at 37°C, lower activity at 22 °C	**BASU**	30 min, 18 hours (Not tested in plants)

3.1.1. Arabidopsis thaliana lines constructed to decipher the protein network regulating CO designation

Execution of successful proximity labelling Mass spectrometry experiment hinges on careful consideration of three factors: (a) functional bait-fusion protein(s), (b) appropriate control(s), and (c) precise exogenous biotin supplementation and labelling duration.

In this study, the following bait proteins (as indicated in Table 3 and Figure 10) were fused to our proximity labelling enzyme to obtain readouts of interacting partners during meiotic crossover designation.

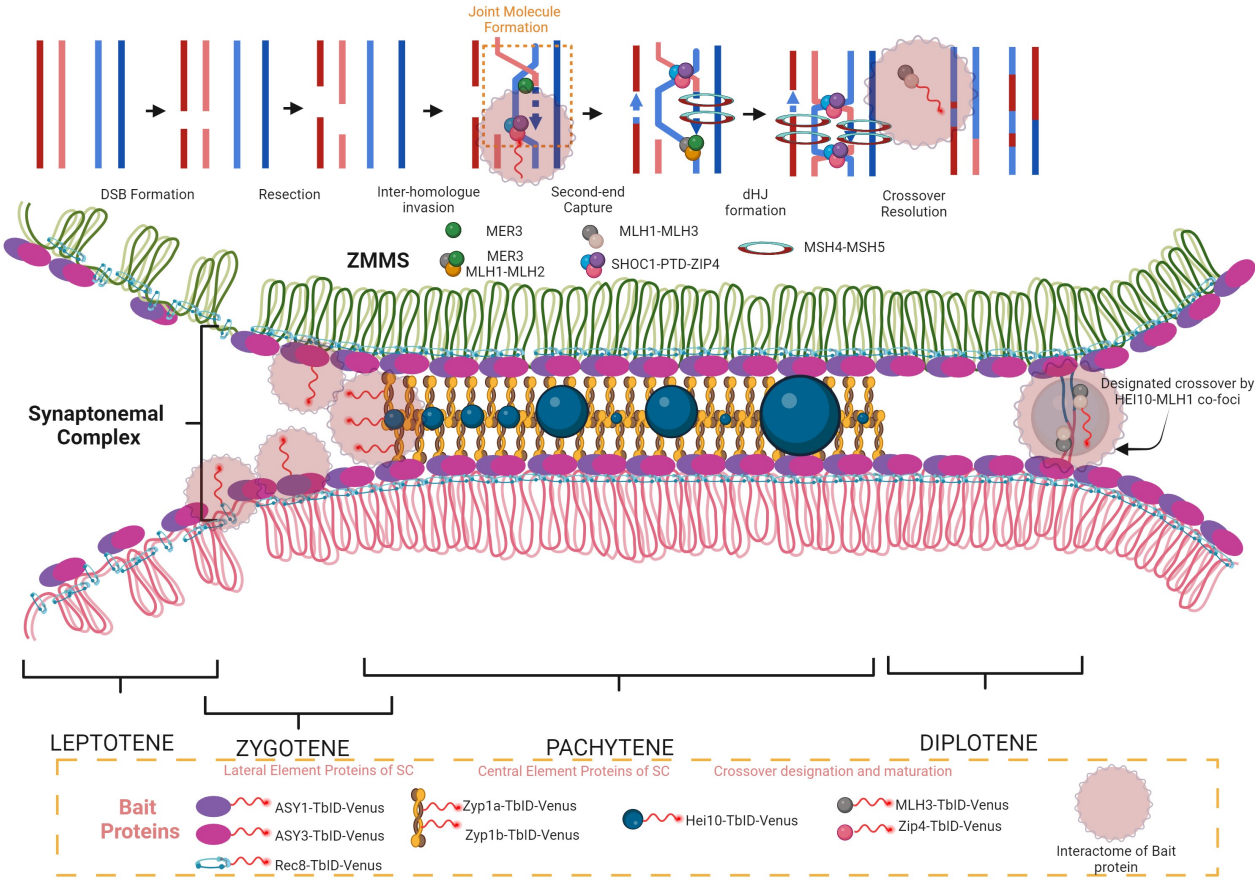

Figure 10| Schematic of Chromosome organisation during meiotic prophase and bait protein employed to capture crossover designation through Proximity labelling. Meiosis commences with the polymerisation of a proteinaceous axis assembled by incorporation of ASY1 and ASY3,

which support the chromatin loops of each homologous chromosome, followed by subsequent zippering of the chromosome axis by transverse filament protein Zyp1A/Zyp1B to form the tripartite SC. This is followed by the programmed induction of DNA DSBs through SPO11, end resection and single-stranded invasion aided by DMC1 and RAD51 to form the D-loop. These joint molecules are then processed as crossovers by the action of the ZMM pathway (MER3, MSH4/MSH5, ZYP1, SHOC1, PTD, ZIP4 and HEI10). Out of the many early recombination nodules, only those which are associated with the formation of large HEI10 foci by late pachytene mature as Crossovers resolved subsequently by the MutLγ MLH1-MLH3.

Construct	Genotype
Controls	
pUBQ10::TbID-YFP-NLS::tNos ($_{UBQ}$TbID-YFP, constitutive nuclear expression of TbID-YFP)	WT
pREC8::TbID-Venus-NLS::tREC8 ($_{REC8}$TbID-Venus, nuclear expression of TbID-Venus driven by REC8 promoter)	WT
pREC8::TbID-Venus-NES::tREC8 ($_{REC8}$TbID-Venus, cytosolic expression of TbID-Venus driven by REC8 promoter)	WT
pMS1::MS1-TbID-Venus::tMS1(MS1-TbID-Venus)	WT
Interactome of Synaptonemal complex lateral elements	
pREC8::REC8-TbID-Venus::tREC8 (REC8-TbID-Venus)	*rec8 (-/-)*
pASY1::ASY1-TbID-Venus::tASY1(ASY1-TbID-Venus)	*asy1 (-/-)*
pASY3::ASY3-TbID-Venus::tASY3 (ASY3-TbID-Venus)	*asy3 (-/-)*
Interactome of Synaptonemal complex central elements	
pZYP1A::ZYP1A-TbID-Venus$_{internal}$::tZYP1A (ZYP1A-TbID-Venus$_{internal}$)	*zyp1-1 (-/-)*
pZYPB1B::ZYP1B-TbID-Venus$_{internal}$::tZYP1B (ZYP1B-TbID-Venus$_{internal}$)	*zyp1-1 (-/-)*
pHEI10::HEI10-TbID-Venus::tHEI10 (HEI10-TbID-Venus)	*hei10-2 (-/-)*
Interactome of Crossover designation and maturation	
pHEI10::HEI10-TbID-Venus::tHEI10 (HEI10-TbID-Venus)	*hei10-2 (-/-)*
pZYP4::ZIP4-TbID-Venus::tZIP4 (ZIP4-TbID-Venus)	*zip4 (-/-)*
pMLH3::MLH3-TbID-Venus::tMLH3 (MLH3-TbID-Venus$_{internal}$)	*mlh3 (-/-)*

Table 4| List of TurboID-tagged bait proteins employed for proximity labelling of meiocytes. The PL enzyme is fused to the bait proteins, which are expressed at endogenous levels driven by their native promoter and terminator. The fluorescent protein Venus is included in the construct to assess protein

localisation and expression. The constructs used as control were transformed in Col-0 background and subsequently selected in T2 to be homozygous for the transgene. The bait proteins were altered in the corresponding mutant background in the Col-0 ecotype and subsequently selected in T2 to be homozygous for both the transgene and the mutant background. REC8, ASY1, and ASY3 were employed to capture the interactome of lateral elements of the SC. The ZYP1 heterodimer constituted by ZYP1A/ZYP1B along with HEI10 which is localised to the central region of the SC was used to probe the SC central region and tagging of the ZMM proteins HEI10, ZIP4 along with the MutLγ resolvase MLH3 were employed to gain insights into Crossover designation and maturation.

Among the ZMM proteins, HEI10 and ZIP4 were chosen as bait proteins. HEI10 was our favoured candidate as progressive coarsening of HEI10 along the SC has been suggested to influence which Early recombination nodules are licensed to form late recombination nodules[43, 49, 86]. Further, the few large HEI10 foci that form at the end of the pachytene after HEI10 coarsening co-localize with MLH1-MLH3, a marker for Class I CO designated sites, which will also shed light on dHJ resolution along with tagging of MLH3. Through tagging of HEI10, we also aim to answer some open questions yet to be explored in this model [78].

We are also interested in the ZMM protein ZIP4 as bait because the ZIP4-SHOC1-PTD complex, through its XPFERCC1-like module, can bind branched recombination intermediates[87, 88]. It has also been shown that ZIP4 interacts with axial element protein ASY3, thus making it an ideal candidate for tagging given its diverse interactions[87].

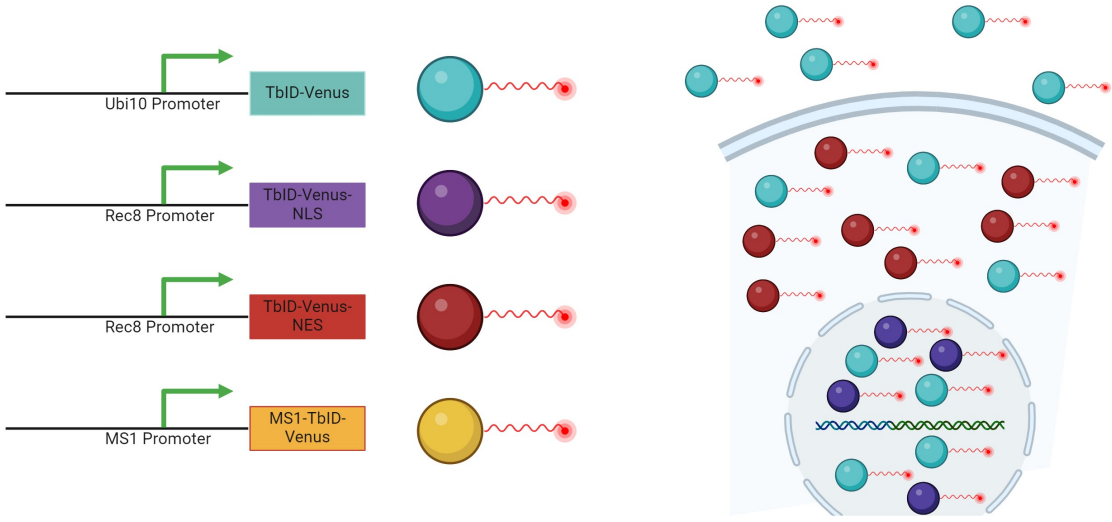

Figure 11| Controls used for Proximity labelling. For filtering out proteins which might be endogenously or stochastically labelled along with weeding out bead-bound nonspecific interactions, we have used the proximity labelling construct driven by the *UBQ10* constitutive promoter as control to map the entire proteome of the bud. To establish the nuclear and cytosolic proteome of meiocytes, the meiosis-specific REC8 promoter was chosen to drive the Proximity labelling construct with an NLS and NES signal peptide. The REC8 promoter was selected as REC8 is expressed right from the premeiotic S phase and persists even after

completion of meiosis I [89]. MS1 tagged Proximity labelling construct was used as a control to filter out noise from the outer layer of somatic cells, namely the tapetum, which envelopes meiocytes [90]

3.1.2. TbID-tagged bait proteins are expressed and localised accurately

To examine whether tagging our bait proteins by the proximity labelling construct yields functional reporter lines, i.e., yields expression of our PL tagged bait protein and shows canonical localisation and expression patterns, live microscopy was employed to follow the bait proteins as they progress through meiosis (Figure 12)

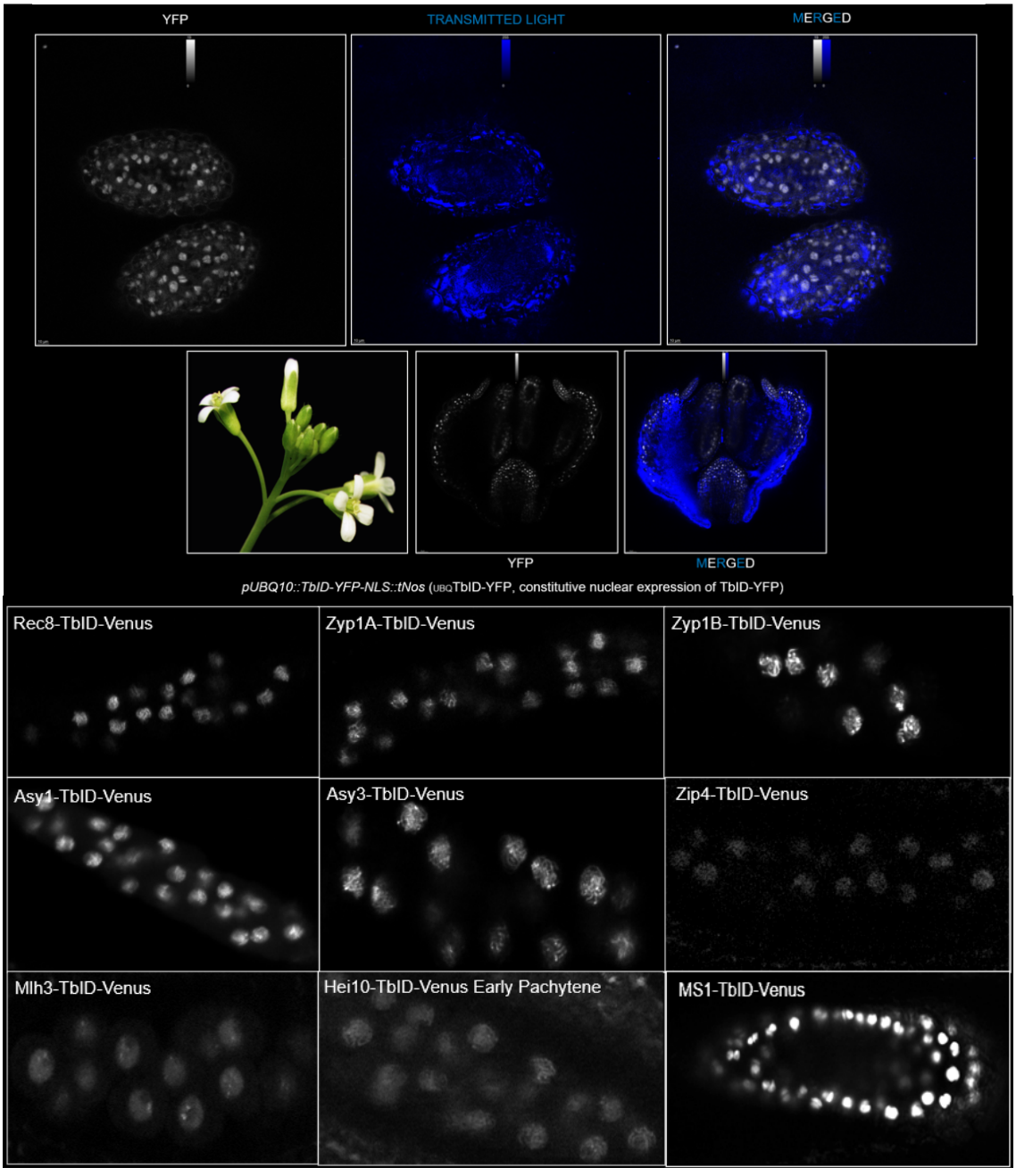

Figure 12| TurboID-tagged bait protein shows accurate expression and localisation profiles. To explore whether tagging our bait proteins doesn't alter their dynamics and behaviour, the bait proteins were followed through mitotic progression by live cell imaging on male meiocytes. As expected, the UBQ10 promoter-driven proximity labelling construct shows constitutive expression throughout the flower bud. Bait proteins which are components of the SC, such as REC8, ZYP1A, ZYP1B, ASY1 and ASY3, appear as

filamentous threads decorating chromosomes. The ZMM protein HEI10 during early pachytene decorates the entire length of chromosome and later forms foci (Not shown). ZIP4 and MLH3 appear as bright puncta only for a brief time window during prophase. MS1 expression is confined to the tapetum

Tagging of the bait proteins with the Proximity labelling construct was observed to increase the half-life of the proteins, resulting in them persisting beyond their canonical expression window in some cases. This might plausibly be due to lower availability of surface exposed lysine residues for Ubiquitination mediated proteasomal degradation due to covalent attachment of biotin to these residues by the proximity labelling enzyme. In case of ZYP1B-TbID, polycomplexes, which are higher order structures of the synaptonemal complex formed independent of chromatin were observed. These might possibly be due to higher expression levels of ZYP1B-TbID transgene promoting the polymerization of polycomplexes. In case of the MLH3 tagged transgenic construct, the expression patterns were unreliable across samples confirmed on several independent transgenic lines. Thus, this construct was dropped for subsequent analysis. For the proximity labelling constructs with an NLS and NES signal peptide driven by the REC8 promoter, no fluorescent signal was detected upon live imaging using the laser scanning confocal microscope (Leica Stellaris 8). Due to the diffuse nature of the expected signal, we assumed the signal to be caught using the more sensitive Airyscan2 microscope (Zeiss LSM 980) but were met by the same outcome. Thus, moving ahead, in order to confirm whether this construct is expressed, RT-PCR needs to be carried out to confirm RNA expression, followed by the detection of proteins by western blotting.

3.1.3. TbID tagged bait proteins biotinylate interacting partners

To assess whether TurboID tagging of our bait proteins could biotinylate interacting partners in vivo, we carried out an anti-biotin western blot on buds harvested from the $_{UBQ}$TbID-YFP constructs. As seen from the western blot, in the presence of exogenous biotin supplementation, we see a clear enrichment of biotinylated proteins. Further, based on immunolocalisations carried out by 3D STED, we see clear biotinylation of the meiotic chromosome axis by REC8-TbID construct. Interestingly, the meiotic chromosome axis also showed biotinylation by REC8-TbID in the absence of exogenous biotin indicating endogenous biotin levels too are sufficient to promote biotinylation of interacting partners.

Figure 13| (Top)Biotinylation of the meiotic chromosome axis in REC8-TbID-Venus. Immunolocalization using an anti-REC8 antibody (Cyan reveals localisation of REC8-TbID-Venus to the meiotic chromosome axis. Immunolocalisation using an anti-biotin antibody (Magneta) was used to assess biotinylation of the meiotic chromosome axis across three groups, Col-0 (Wild type control) with the absence of the proximity

labelling construct and REC8-TbID-Venus plants across two treatments, namely H20 and 0.5mM Biotin. REC8-TbID-Venus results in biotinylation of the meiotic chromosome axis even in the absence of exogenous biotin.

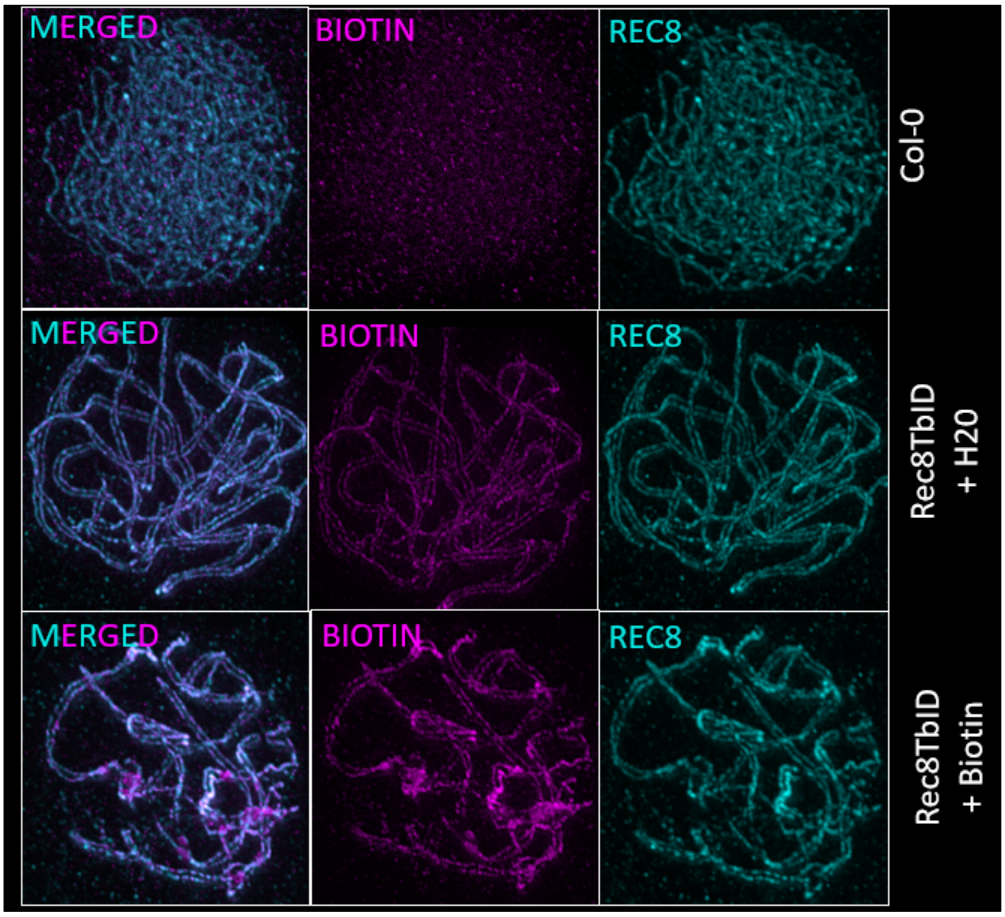

(Bottom)Biotinylation in UBQ-TbID-Venus plants. Immunoblot on total protein from 50 dissected flower buds containing cells undergoing meiosis (≤0.5mm). 2, 2', 4, 4' were treated with exogenous biotin of 0.2 mM for overnight. 1',2', 3', 4' was probed using an anti-biotin antibodywhich is more sensitive in the detection of biotinylated proteins, while 1,2,3,4 was probed using HRP conjugated Streptavidin. Below panel is sample controls using anti-Histone H3 antibody (Expected band at ~15KDa)

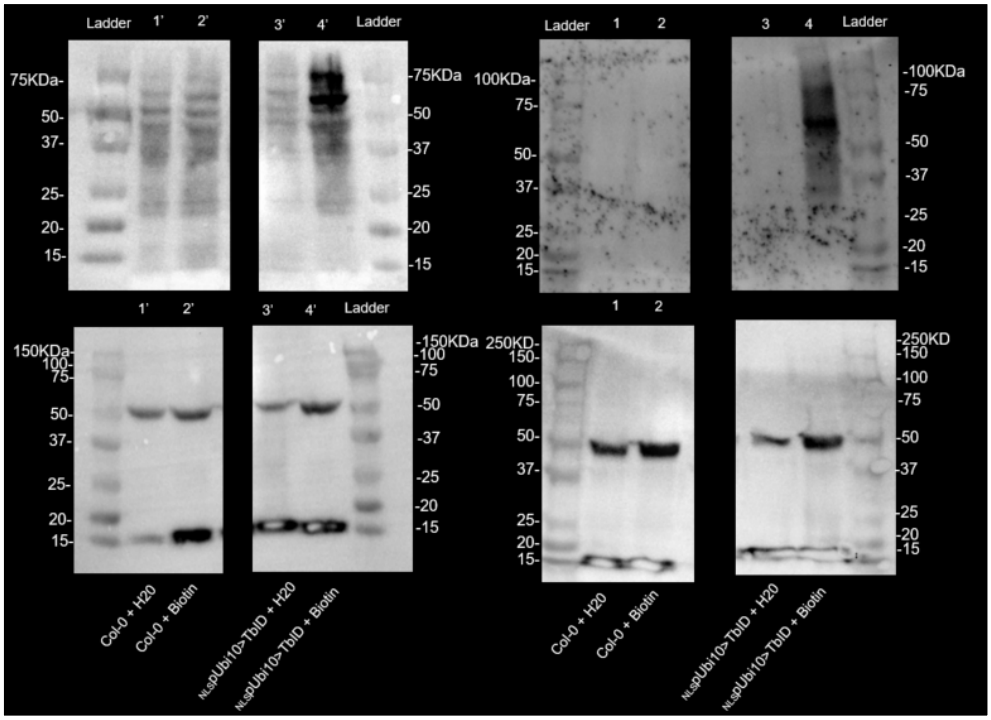

3.1.4. Complementation of TbID tagged bait proteins

To assess if tagging our bait proteins with TbID interferes with their role in normal meiotic progression, these transgenic lines were phenotypically studied and compared to the corresponding null mutant backgrounds of the bait proteins and WT plants. No visible differences were seen in vegetative growth and development for any of the transgenic lines. UBQTbID-Venus plants showed a ~21% reduction in fertility compared to WT plants, possibly due to the constitutive expression of the proximity labelling construct throughout the plant tissue.

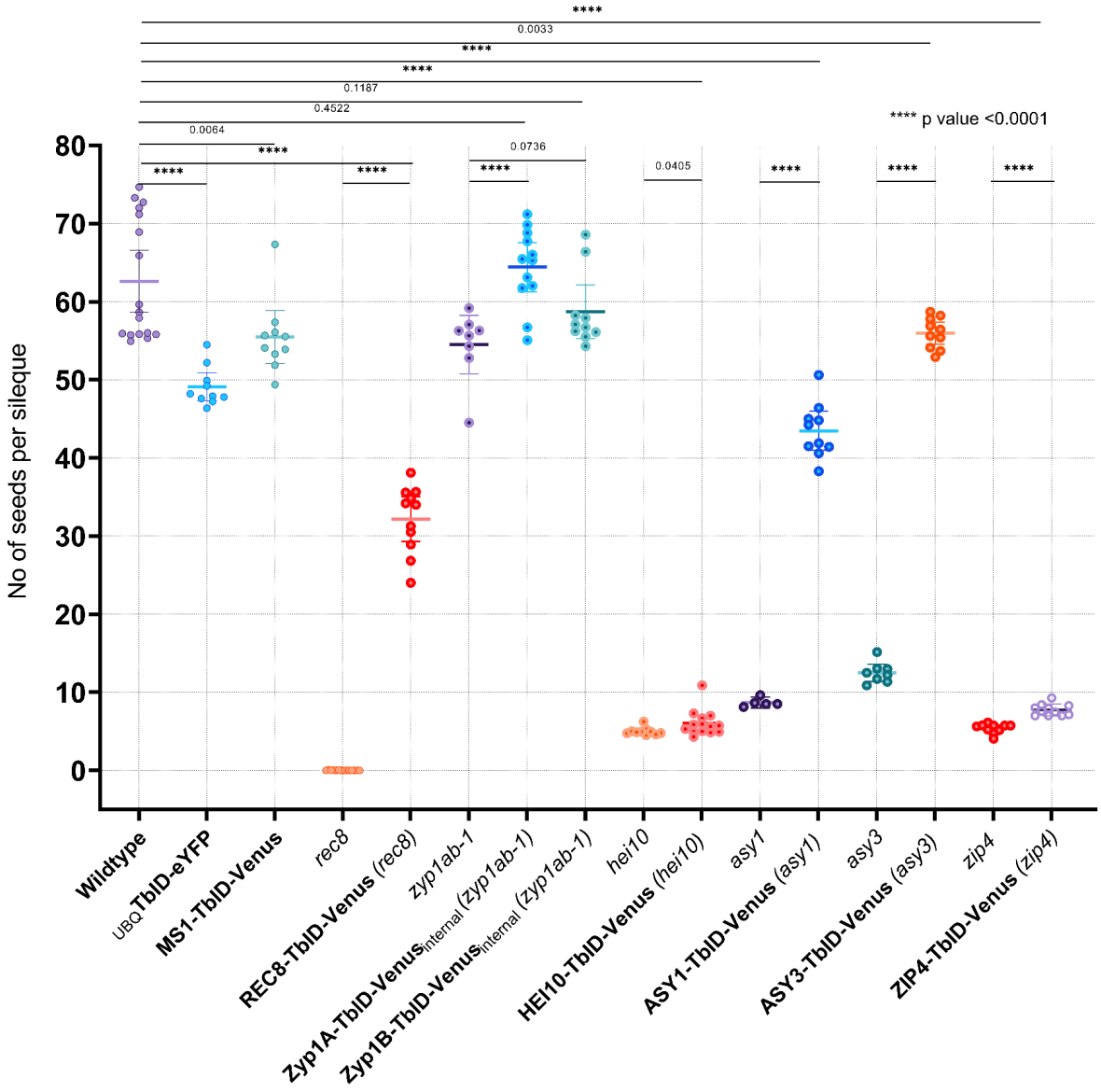

Figure 14| Quantification of seeds per silique to assess fertility of TbID tagged baits. Data are presented as mean ± standard deviation (S.D). Col-0 (62.6±7.5), $_{UBQ}$TbID-eYFP (49.1±2.3), MS1-TbID-Venus (55.4±4.5), REC8-TbID-Venus (32.2±4.1), *rec8-3* (0.01±0.02), ZYP1A-TbID-Venus (64.4±4.8), ZYP1B-TbID-Venus (58.7±4.5), *zyp1ab-1* (54.5±4.2), HEI10TbID-Venus (6.0±1.6), *hei10-2* (5.0±0.4), ASY1-TbID-Venus (43.5±3.3), *asy1-4* (8.6±0.5), ASY3-TbID-Venus (56.0±1.9), *asy3-1* (12.5±1.2), ZIP4-TbID-Venus-(7.7 ± 0.7), *zip4-2* (4.8±0.5). Each circle represents the average number of seeds per fruit from one plant, obtained by

counting at least ten fruits per plant. The mutant background of the bait protein is compared to the corresponding genotype where the TbID fused bait protein is introduced on a T-DNA. ****P < 0.0001, ****P<0.001, NS, not significant.

When the proximity labelling construct was expressed in a cell type-specific manner, as seen in the case of MS1-TbID-Venus, whose expression is confined to the tapetum, the reduction in fertility was a marginal ~11% compared to WT levels. REC8-TbID-Venus plants complement the *rec8* mutant by restoring fertility by ~50% compared to WT levels as opposed to no seeds seen in *rec8* plants, suggesting partial complementation. ZYP1A-TbID-Venus showed fertility similar to WT plants, suggesting complementation. However, ZYP1B-TbID-Venus plants showed ~6% decrease in seed number per sileque compared to WT levels. This can be explained by the appearance of polycomplexes, a complex network of abnormal SC-like structures [91], observed in ZYP1B-Tb-Venus plants upon live imaging of male meiosis. ASY1-TbID-Venus and ASY3-TbID-Venus, both restore fertility by ~80% in comparison to corresponding null background of *asy1* [92] and *asy3* respectively. However when compared to WT plants ASY3-TbID-Venus restores fertility by ~90% suggesting complementation as opposed to ASY1-TbID-Venus where we see ~70% fertility compared to WT plants which suggest partial complementation. HEI10-TbID-Venus and ZIP4-TbID-Venus showed fertility levels similar to *hei10* and *zip4* mutants, respectively, indicating a lack of complementation. This could either be due to self-biotinylation of the bait proteins impeding protein function or tagging at the C-terminal domain of these proteins impeding with protein function.

3.1.5. C-terminal tagging of REC8 leads to premature depletion in pericentromeric cohesion during Meiosis I

In REC8-TbID-Venus as previously mentioned we saw partial complementation in comparison to *rec8* mutant background where we recovered 50% fertility compared to WT plants. To investigate this further, we carried out male meiotic chromosomal spreads in REC8-TbID-Venus. Meiotic chromosomal spreads revealed that the progression of meiosis in REC8-TbID-Venus is similar to the wild type till Metaphase I. During Metaphase I in WT, five bivalents align on the metaphase plate (Figure 15a), indicating homologous chromosomes being connected by a chiasmata. In REC8-TbID-Venus, five bivalents were recovered during Metaphase I (n=18), indicating normal CO formation (Figure 15e). In WT plants, the five bivalents at

metaphase I subsequently separate at anaphase I, resulting in two distinct groups, each having 5 chromosomes on opposite sides of the organelle band. Subsequently, the two sets of 5 chromosomes align and separate in metaphase II and anaphase II, respectively, generating four sets of 5 haploid chromosomes each (Figure 15b). In REC8-TbID-Venus following metaphase I, the chromosomes fail to segregate faithfully resulting in unbalanced chromosomes in the dyad of cells post meiosis I with 11 and 9 chromosome (Figure 15f). These chromosomes further segregate randomly segregate at anaphase II (Figure 15f) (n=2) suggesting premature depletion of pericentromeric REC8 pool during Meiosis I. This is further supported by the fact that REC8-TbID-Venus seems to phenocopy *atsgo1-2* [93] where there is early depletion of pericentromeric REC8 due to lack of protection conferred by SGO . However unlike *rec8* mutants, univalents and chromosome fragmentation was not observed during metaphase I along with detection of chromatin bridges [94] suggesting REC8-TbID-Venus behaves like a leaky *rec8* mutant with rescue in chromosome fragmentation phenotype as observed in the corresponding null mutants however shows early loss in pericentromeric cohesion possibly due to C-terminal tagging.

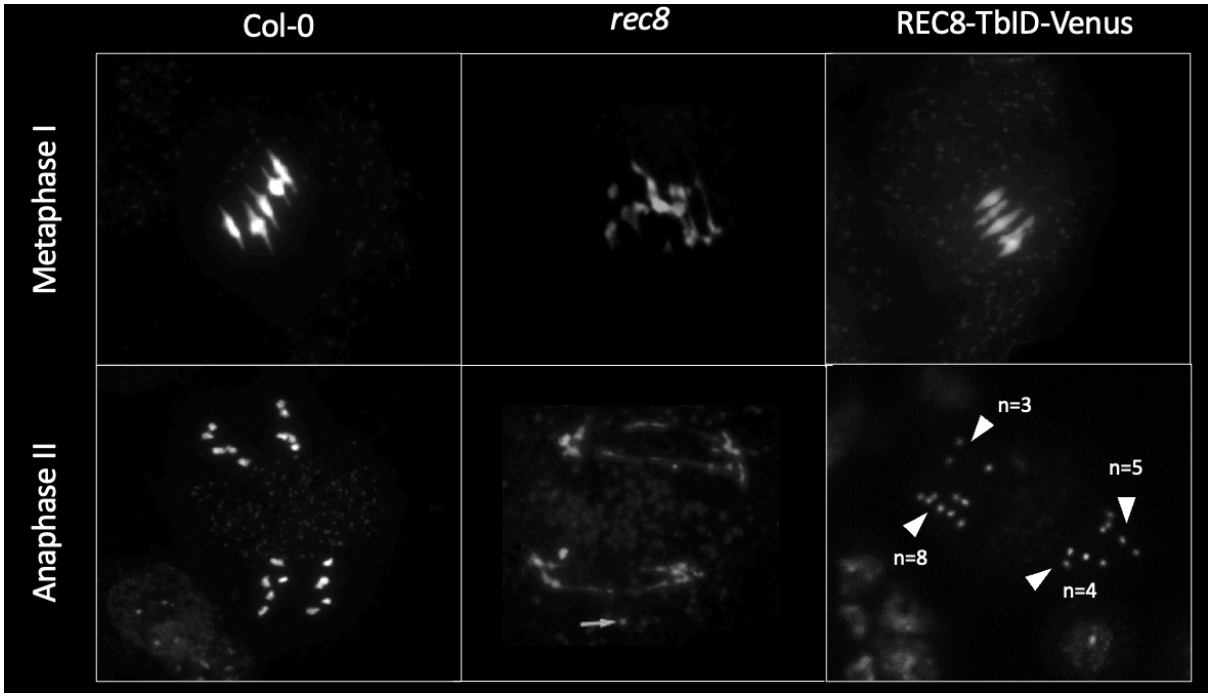

Figure 15| Male meiotic chromosomal spreads of Col-0 WT and REC8-TbID-Venus. Meiotic spreads of WT (a,b), *rec8* (c,d) and REC8-TbID-Venus (e,f). Metaphase I (a,c,e) and Anaphase II (b,d,f). *rec8* spreads courtesy [94]

3.1.6. TbID-based proteomic profiling of chromosome axis in REC8-TbID-Venus

A total of 300 inner inflorescences (≤0.5 mm) from young flower buds were dissected for REC8-TbID-Venus, $_{UBQ}$TbID-Venus and Col-0, with and without biotin treatment for REC8-TbID-Venus and Col-0 and only biotin treatment for $_{UBQ}$TbID-Venus (with two replicates for each treatment). These were then used for protein affinity purification and mass spectrometry analysis. Statistical analysis was performed with MaxQuant search and quantified by LFQ intensity (label-free quantification) to compare between samples. Data analysis was performed using standard analysis, which compares if a protein is found in one condition but not in the other, indicating enrichment. Standard analysis was performed by comparing WT samples treated with biotin and water, which showed no significant difference between the two treatments, barring the gene ZEUS1 (pink dot in Figure 16a) which instringly encodes ta hymidylate kinase having functions in gametophytic to sporophytic transition post fertilization[95]. No other prominent differences were observed between the two groups barring ZEUS1 and subsequently, all groups were compared with WT samples treated with biotin for standard analysis. Standard analysis was then performed by comparing $_{UBQ}$TbID-Venus vs WT samples and REC8-TbID-Venus vs WT samples, and volcano plots were generated (Figure 16b and 16c). From the volcano plots for biotin-treated UBQTbID-Venus vs WT, we see a clear enrichment of biotinylated proteins, indicating efficient biotin conjugation by our TbID construct. However, on comparison of biotin-treated REC8-TbID-Venus vs WT we do not see any enrichment of peptides specific to known interacting partners of REC8 such as other condensins and cohesins (which serve as positive control for our experiment) suggesting that the tissue processed was not sufficient to capture enough cells in the right stage where REC8 is expressed . However interestingly REC8-TbID-Venus is shows up in the list of enriched peptides with a -logP value of 1.6 and enriched ~235 times more in comparison to our control. This possibly might be due to the fact that while generating the transgenic REC8-TbID-Venus line there might have been several tandem insertions of the transgenes as normally is reported for *Agrobacterium* transformation, resulting in its higher expression levels and enrichment of peptides. Moving ahead to successfully capture the proteome of the chromosome axis by proximity labelling using our REC8-TbID-Venus line, we will need to optimize biotin treatment further and overcome the limitations posed by the limited availability of meiotic cells in our sample, resulting in peptides being below

the detection limit of MS. Alternatively one could also use a more sensitive Mass spectrometric approach to capture these peptides.

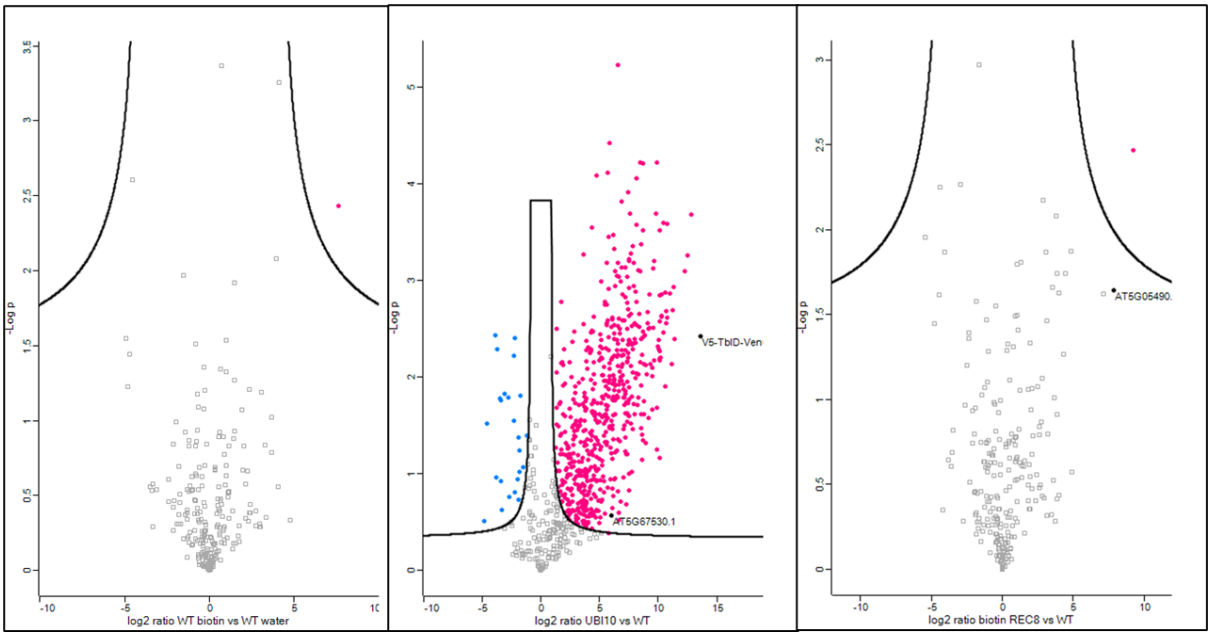

Figure 16| Volcano plots depicting identified candidates and their enrichment through MS analysis. Comparison between WT samples (Col-0) with and without biotin treatment, $_{UBQ}$TbID-Venus vs WT (Biotin treated) and REC8-TbID-Venus (Biotin treated) vs WT (Biotin treated)

Gene Name	Gene ID	Peptides	Unique pepti	Sequence coverage [%]	Q-value	Score	MS/MS count	log2 ratio biotin REC8 vs WT	-log p value
DEAD box RNA helicase 1	AT3G01540	5	3	10	0	323.31	11	**9.24809742**	2.466038
alpha/beta-Hydrolases superfamily protein	AT5G51180	2	2	4.8	0	78.596	1	2.912508965	2.1744652
lipid transfer protein 6	AT3G08770	1	1	9.7	0.0078125	5.8601	1	3.834827423	2.0802946
Lactate/malate dehydrogenase family protein	AT5G43330	2	2	7.5	0	11.544	2	4.829157829	1.87178819
acetyl Co-enzyme A carboxylase biotin carboxylase subunit	AT5G35360	1	1	4.4	0	9.2557	2	3.081725121	1.8669566
Heat shock protein 70 (Hsp 70) family protein	AT5G42020	2	2	5.7	0	37.925	3	3.859408379	1.74165865
Protein of unknown function DUF1395 (InterPro:IPR009829)	AT3G60660	1	1	4	0	57.291	3	4.438063622	1.7400483
Ribosomal protein L18e/L15 superfamily protein	AT5G27850	1	1	5.9	0	6.5581	4	3.509231567	1.65719897
Rad21/Rec8-like family protein	AT5G05490	6	6	14.1	0	323.31	15	7.876448631	1.64429441
Enolase	AT2G36530	1	1	3.8	0.0075758	5.8104	1	3.972967148	1.62937831
plant U-box 49	AT5G67530	3	3	6.1	0	34.823	4	7.168639183	1.62131051
S-adenosylmethionine synthetase 2	AT4G01850	2	2	5.1	0	20.492	3	3.135306358	1.460626

Table 5| List of enriched peptides upon MS analysis REC8-TbID. Upon Biotin treatment and subsequent MS analysis of REC8-TbID plants, the following peptides were enriched when compared to WT control, $\log_2$(REC8 Biotin vs WT)>1.5, -$\log_2$(p value)>1.5

3.2. Functional characterisation of different domains of HEI10 governing CO patterning

Human enhancer of Invasion 10(HEI10) is a conserved eukaryotic ZMM protein required for class I CO in several species. HEI10 is a member of the Zip3/HEI10 broad family of proteins, which can be divided into two main subgroups: the HEI10/CCNB1IP1 family and the Zip3/RNF212 family[34]. HEI10 encodes an E3 ubiquitin ligase that possesses a RING (Really Interesting New Gene) domain characterised by a C3H4 structure which typically recruits E2 ubiquitin-conjugating enzymes and direct transfer of ubiquitin from E2 to the substrate with the remaining part of RING-type E3 ligase enabling substrate recognition[96]. Recent studies have suggested that HEI10 may play an essential role in crossover designation through a diffusion-mediated coarsening process [43, 49]. By late prophase, few large HEI10 decorate chromosome and form a co-foci with MLH1, facilitating the final stage of CO maturation.In *Sordaria macrospora* HEI10 acts as a central hub integrating signals from several players involved in meiosis to facilitate formation of recombination complexes through ubiquitination and SUMOylation processes [97]. Despite the structure of HEI10 proteins being highly conserved, the role of RING domain in plant HEI10 proteins and its function as a E3 ligase is unclear.

3.2.1 HEI10 alleles to study role of RING domain and HEI10 tetramerization

Despite the crucial role played by HEI10 dosage for crossover formation [48], its biochemical activity and functional characterisation of its different domains driving its coarsening dynamics along the SC in plants is still poorly understood. To probe the role of the RING domain in plant HEI10 and its role for HEI10 dynamics, the Leucine 23 and Leucine 45 residues were mutated to Aspartic Acid (L23D L45D), suggested to kill the RING activity of HEI10 based on structure predictions by Alphafold2 and comparing the homology of Arabidopsis HEI10 to equivalents in humans and *S. cerevisiae* (Figure 17) (Courtesy collaborations with, John Weir and Raphäel Guerois). Alphafold2 simulations also suggest HEI10 to exist as a tetramer, and mutating the Leucine 74 residue is predicted to disrupt the ability of HEI10 to form a tetramer (Figure 17). To probe whether Alphafold2 predicted tetramerisation of

HEI10 is dispensable for its functioning, the Leucine 74 was mutated to Glutamic acid (L74E).

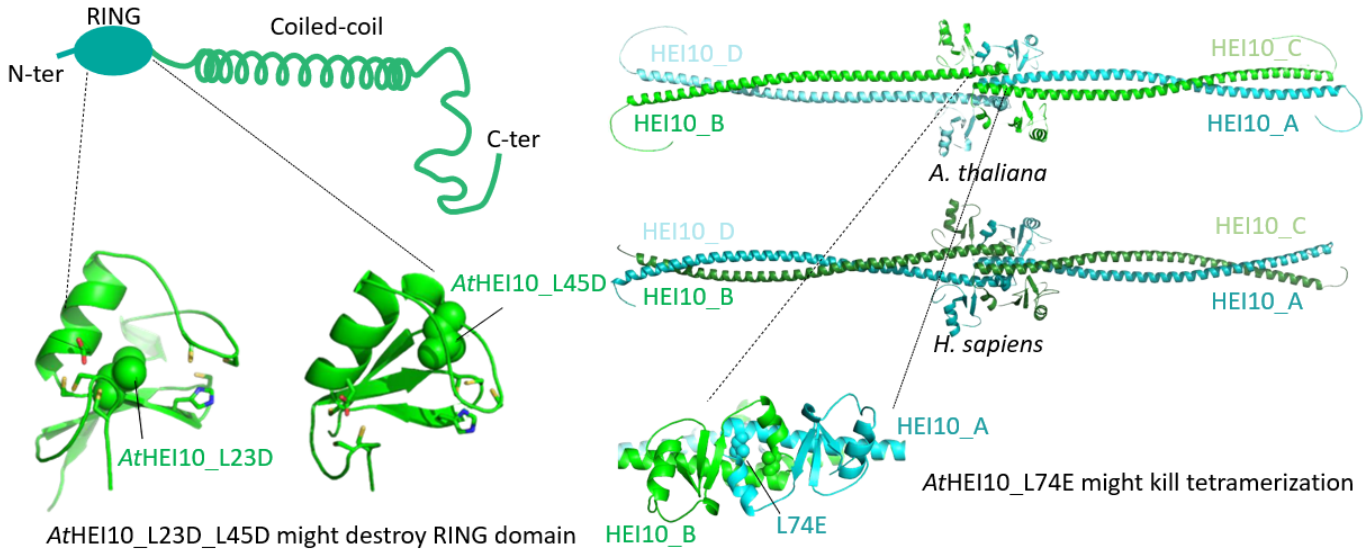

Figure 17| Mutations to kill RING domain and predicted tetramerisation of HEI10 based on Alphafold2 simulations. (Right) Schematic representation of HEI10 indicating its N-terminal RING domain, followed by a coiled-coiled domain and C-terminal intrinsically disordered domain. A zoomed view of the RING domain is presented to highlight the amino acids Leucine23 and Leucine45 predicted to kill E3 ligase activity of HEI10 based on Alfphafold2 modellnig. (Left) Alphafold2 predicts HEI10 to exist as tetramers due to interactions facilitated by the Leucine74 residue whose mutation to Glutamic acid is suggested to disrupt this tetramerization.

The mutant alleles of *HEI10* were cloned with mutations being confirmed by Sanger sequencing (Figure 18) and transformed in *hei10-1* mutant background (*WS-4* ecotype) and subsequently selected for the presence of *HEI10* allele introduced as T-DNA in a *hei10* null background by genotyping T1 plants.

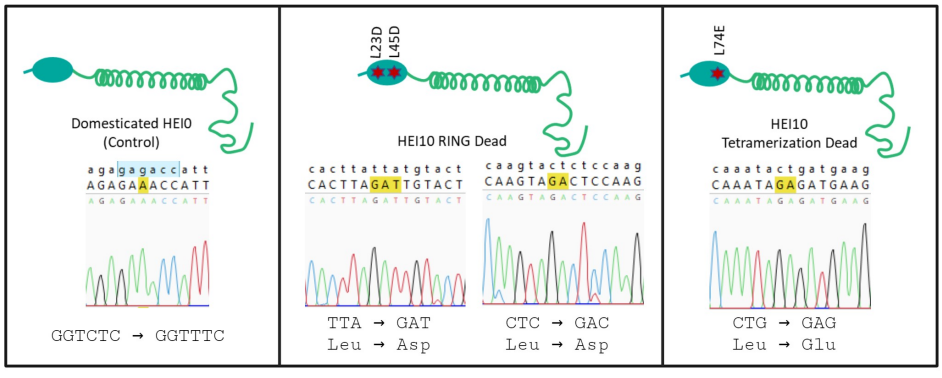

Figure 18| Sanger sequencing chromatograms confirming mutations in *HEI0* alleles. Illustration showing HEI10 and respective amino acids mutated in the different alleles. *HEI10* with a synonymous mutation in the B*sa*I recognition site GGTCTC was used as a control. In the HEI10 RING dead allele, the TTA codon corresponding to Leucine 23 and CTC codon corresponding to Leucine 45 are mutated to GAT and GAC, respectively coding for Aspartic acid. In the HEI10 TETRA dead allele, the CTG codon coding for Leucine 74 is muated to GAG coding for glutamic acid.

3.2.2 Complementation of HEI10 alleles

Complementation of the different *HEI10* alleles was assessed by examining the fertility (seeds per silique) by comparing to *hei10-1* plants heterozygous for a functional *HEI10* allele as the analysis was done on T1 plants with a single copy of *HEI10* transgene. Introduction of a wildtype *HEI10* allele as a transgene in a null *hei10* background complements resulting in WT levels of fertility. However, the *HEI10 RING Dead* allele fails to complement *hei10-1* mutants (Paired T-test, $P<10^{-4}$, Figure 19), indicating the indispensable role of the RING domain for crossover formation in *Arabidopsis* based on preliminary evidence. Failure of the RING domain mutant of HEI10 to complement suggests that this domain is essential for HEI10 function plausibly by regulation of ubiquitination/SUMOylation, we speculate. *HEI10 TETRA DEAD* also fails to complement *hei10-1* mutants, suggesting that higher-order interactions of HEI10 are indispensable for its function. An exciting hypothesis to explain this might be that HEI10 in its oligomeric state serves as a scaffold favouring multivalent interactions thereby promoting HEI10 coarsening in conjunction with the SC which has been shown to exhibit liquid crystal like behaviour in Caenorhabditis elegans[98]. However, this needs repeated to make claims with statistical significance and meiotic progression in these mutants needs to be examined cytologically by immunofluorescence. Further we need to validate these genetic data with biochemical assays and future research should be conducted in this direction.

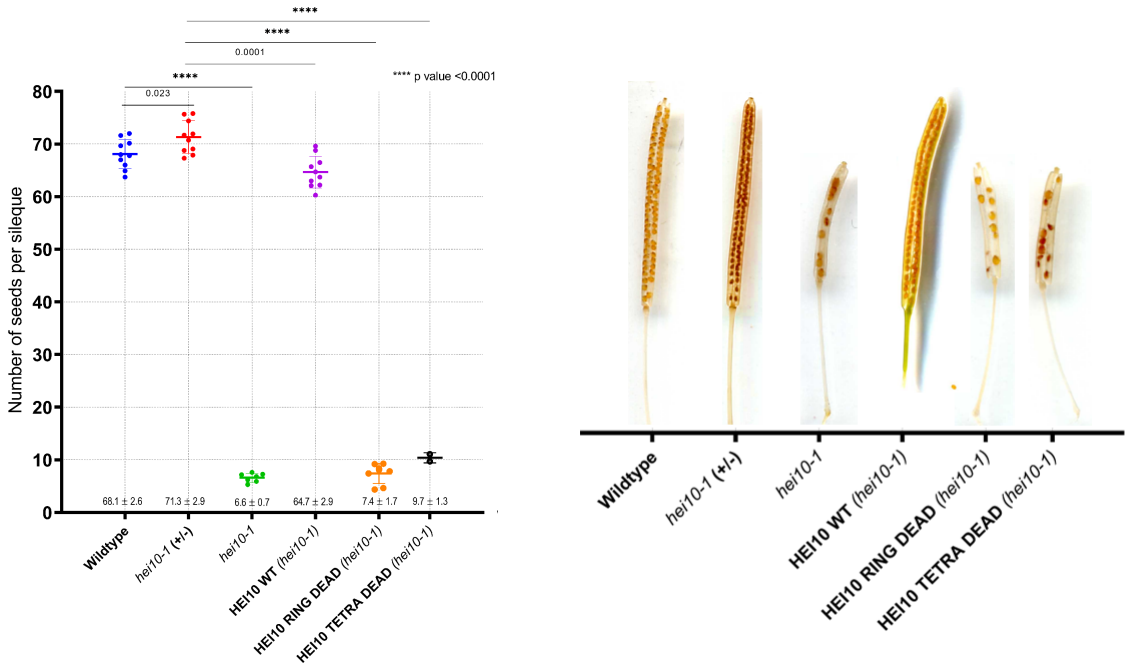

Figure 19| Complementation of *HEI0* alleles. Data are presented as mean ± standard deviation (S.D). WT (68.0±2.6), *hei-1* (het) (71.3±2.9), *hei10-1* (6.6±0.7), *HEI10 WT* (64.6±2.8) *HEI10 RING DEAD* (7.4±1.7),

HEI10 TETRA DEAD (9.7±1.3). Each circle represents the average number of seeds per fruit from one plant, obtained by counting for at least ten fruit per plant. *HEI10* alleles are compared to *the hei-1 mutant genotype with heterozygous and wildtype sister plants cultivated* from a segregation population. Representative cleared fruits of *hei10-1* controls and *HEI10* alleles are shown. Wild-type *HEI10* allele introduced as a T-DNA complements *hei10-1* plants.

3.2.3 CRISPR-Cas9 gene editing targeting different domains of HEI10 to assess their role for HEI10 function

Arabidopsis thaliana HEI10 is encoded by the At1g53490 locus. The gene has ten exons with the CDS starting from the third exon to the tenth exon coding for a full-length protein which is 304 amino acids in length. HEI10 has a conserved N-terminal RING domain (C3HC4 zinc finger), followed by a central coiled-coiled region and an intrinsically disordered domain at the C-terminal of the protein (Figure 20).

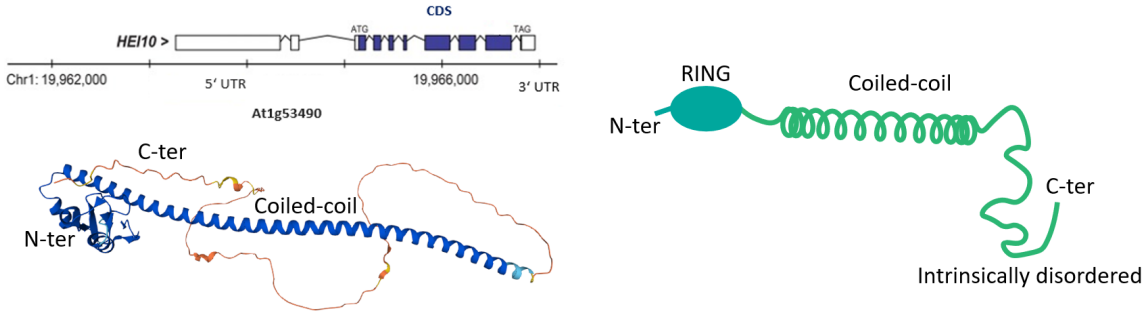

Figure 20| HEI*0* locus on chromosome 1 along with Alphafold2 structure prediction of HEI10. *HEI0* is located on the At1g53490 locus on chromosome 1 with the coding sequence shown in blue with the position of the start and stop codon indicated. The *Alphafold* structure prediction of HEI10 is indicated below along with a cartoon representation HEI10 structure.

To assess the function of the Coiled-coiled domain of HEI10 and generate different alleles of the intrinsically disordered C-terminal tail of HEI10 shown to be important in regulating HEI10 loading and coarsening along the SC courtesy previous work in our lab (unpublished), we designed sgRNA's targeting the coiled-coiled domain and C-terminal tail which were transformed in WT plants. sgRNA were also designed to generate a *hei10* deletion line in Col-0 ecotype.

An allele of *HEI10* having a 403 bp deletion was recovered on screening T2 plants for deletions in the coiled-coiled domain (Figure 21). However, the deletion detected was out of frame limiting subsequent analysis.

Figure 21| Deletion of *HEI10* coiled-coiled domain by CRISPR-Cas9 editing. Schematic representation of *HEI10* locus indicating regions targeted by CRISPR-Cas9. The promoter and terminator are indicated in Red. sgRNA are represented by magenta, followed by the adjacent protospacer motif in blue and predicted cut sites shown by triangles. Partial sequences of individual deletions are shown with distance between

adjacent sequences denoted by n. The ORF is indicated by a rectangle. The size of the deletion is indicated below which is a frameshift deletion.

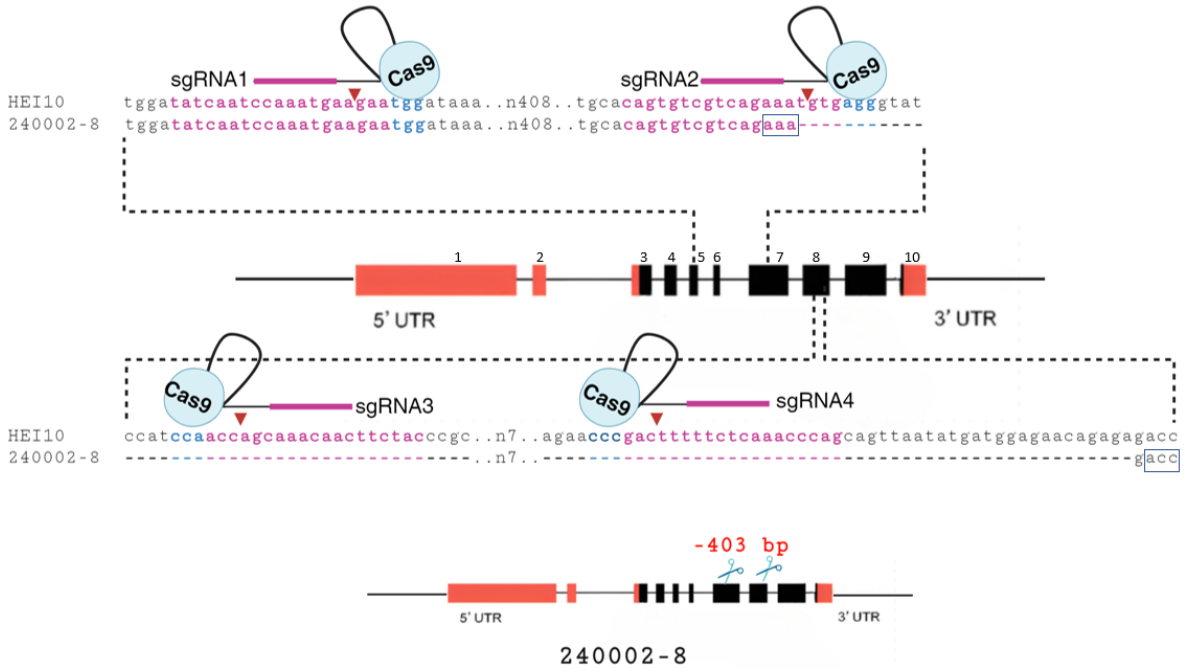

On screening lines for deletions in the C-terminal tail of *HEI10,* we were able to recover three independent deletions lines (Figure 22). 240033-3 had an in-frame deletion of 6bp in the ninth exon followed by 709 bp deletion removing the tenth exon containing the stop codon. However, one codon downstream of the cut there is a stop codon UGA which could potentially be used to produce a truncated protein but needs to be validated further. 240006-31 had an 839 bp deletion removing the seventh, eight and part of the ninth exon coding for the coiled-coiled domain and part of the C-terminal tail. However, the deletion recovered is a frameshift deletion. Moving ahead if we manage to recover an in-frame deletion removing the coiled-coiled domain and C-terminal tail of HEI10, retaining only the RING domain, it would be interesting to check this deletion line complements the HEI10 RING dead mutant by crossing to it.

Figure 22| Deletion of *HEI10* C-terminal domain by CRISPR-Cas9 editing. Schematic representation of *HEI10* locus indicating regions targeted by CRISPR-Cas9. The promoter and terminator are indicated in Red. sgRNA are represented by magenta, followed by the adjacent protospacer motif in blue and predicted cut sites shown by triangles. Partial sequences of individual deletions are shown with distance between adjacent sequences denoted by n. The ORF is indicated by a rectangle. The size inframe (green) and frameshift (red) deletions are indicated below for the corresponding lines.

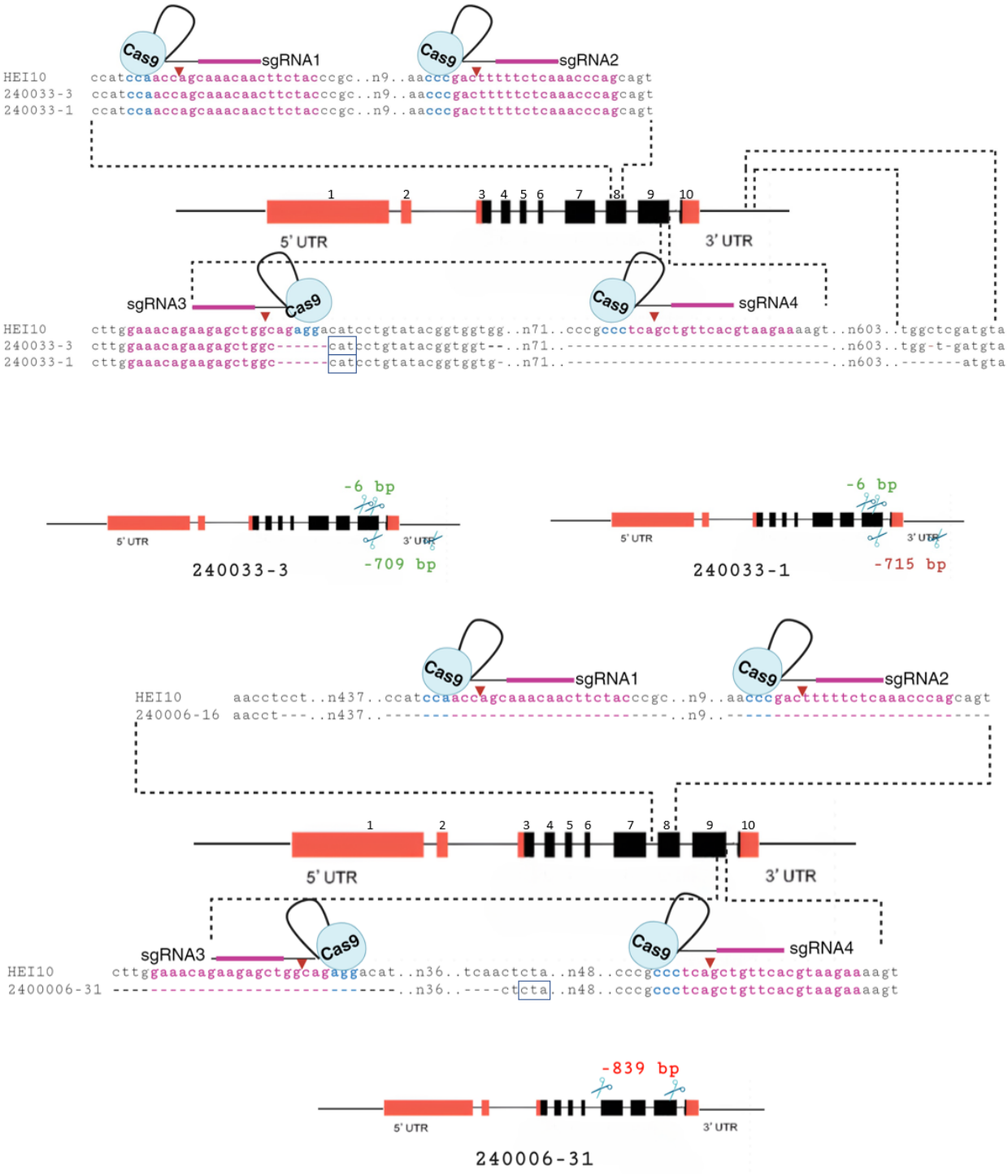

We were successful in generating two independent deletion lines of *HEI10* by CRISPR-Cas9 gene editing in Col-0 ecotype. 240055-2 was 2427 bp deletion 270 bp upstream of the start codon and removing the CDS completely. 240032-5 was a 2178 bp deletion 11 bp upstream of the start codon and removing the CDS too. However, in 240032-5 part of the *HEI10* promoter is still present making 240055-2 a better choice for a *hei10* null background for future studies in Col-0 ecotype.

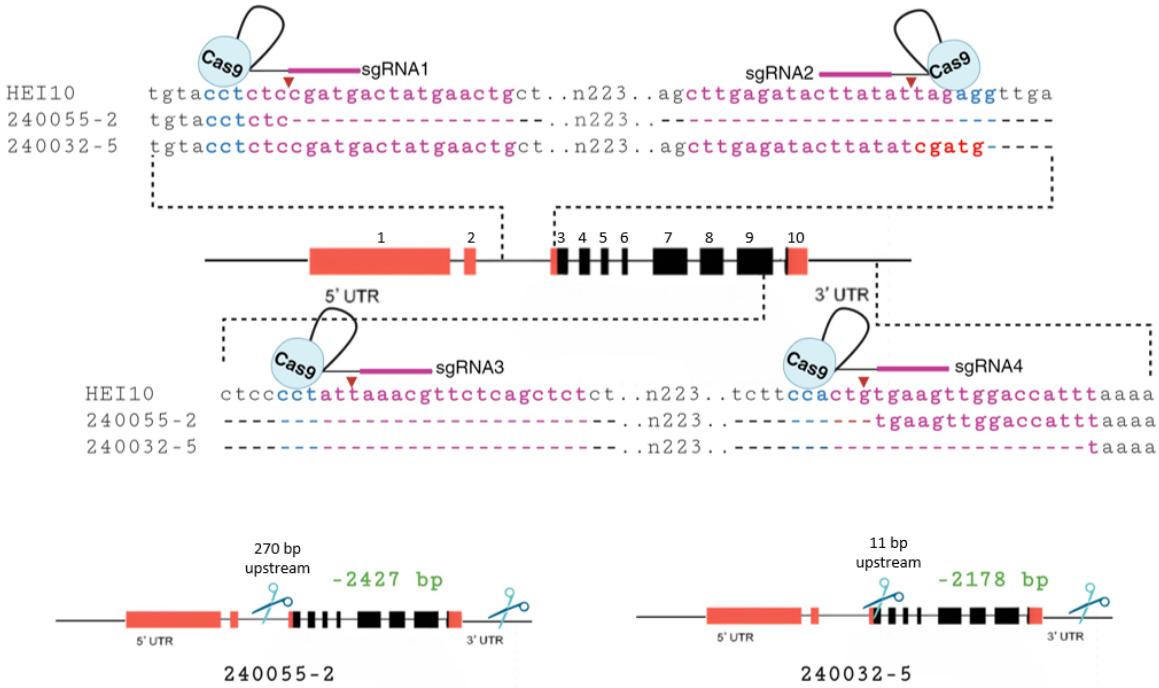

Figure 23| *HEI10* null alleles generated by CRISPR-Cas9 editing. Schematic representation of *HEI10* locus indicating regions targeted by CRISPR-Cas9. The promoter and terminator are indicated in Red. sgRNA are represented by magenta, followed by the adjacent protospacer motif in blue and predicted cut sites shown by triangles. Partial sequences of individual deletions are shown with distance between adjacent sequences denoted by n. The ORF is indicated by a rectangle. The of the deletions are indicated below for the corresponding lines.

To examine for chromosome translocation associated with CRISPR-Cas9 gene editing, Alexander staining [84] was performed to assess for dead pollen commonly associated with translocations. For both the *hei10* deletion lines no dead pollen was detected and these *hei10* null alleles generated in Col-0 ecotype will serve as a useful line for future complementation studies in a null *hei10* background.

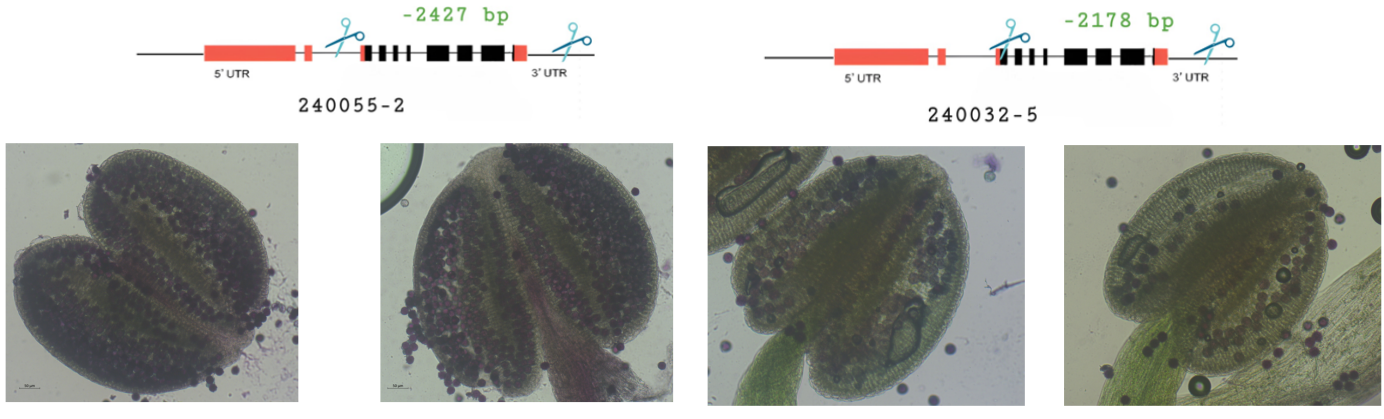

Figure 24| Alexander staining to assess pollen viability for *hei10* deletion lines. Alexander stainig allows for distinction between viable and non-viable (sterile,aborted) pollen based on differential staining. Viable pollen is stained purple while non-viable pollen is stained pale turquoise. For the both the *hei10* deletion lines the pollen was viable (purle) indicating lack of translocatins.

Chapter 4 Concluding remarks and future outlook

In *Arabidopsis thaliana* so far ~80 gene have been identified to be involved in meiosis. Out of these, 28 genes are exclusive to meiosis and the other 51 genes are involved in meiosis as well as DNA repair of somatic cells (Christine Mézard, unpublished). These genes have been identified by different screens such as a forward genetic screen, reverse genetic screen or suppressor screen (Figure 25)

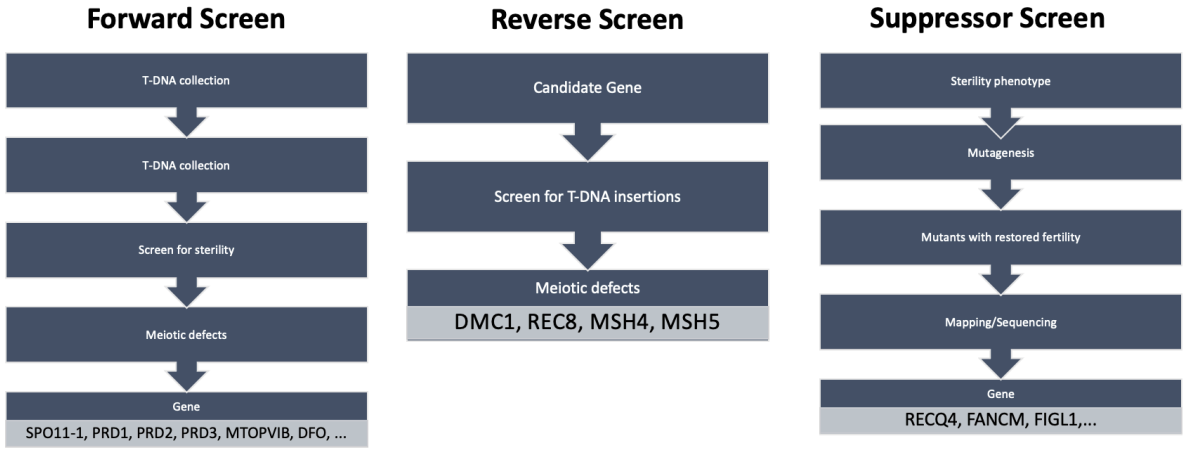

Figure 25| **Genetic screens to identify meiotic genes.** The following three screening strategies namely, forward genetic screen, reverse genetic screen and supressor screens have traditionally been used to identify novel meiotic genes in *Arabidopsis thaliana.* Courtesy Christine Mézard

Using the following screening strategies one can only identify meitotic genes giving strong phenotypes such as complete or drastic reduction in fertility due to formation of aneuploid gametes, or restroration of fertility (from severe sterility in supressor screens) or cytological detected abberations in meiotic progression as seen using DAPI chromosomal spreads leading to univalents and chromosome fragmentation phenotypes in mutants. However, these genetic screens do not capture meiotic genes which produce a mild phenotype or those genes which exist as several copies due to duplication events and are often not disrputed by mutagenesis. Thus to identify novel actors which regulate meiosis, in particular during crossover designtion, we have resorted to the proteomic approach of proximity labelling where meiotic genes / components known to regulate crossover distribution along chromosomes are used as bait proteins by tagging them with the proximity labelling enzyme TurboID (TbID). This approach equips us to fish out new unexplored players which regulate this process. To this end, we have generated several transgenic lines where the meitoic specific bait proteins were tagged with the proximity labelling

enzyme and their complemenation was assesed. Further using western blotting, immunoflorescence microscopy and MS analysis we have confirmed the ability of these constructs to biotinylate interacting partners in-vivo. However some standardization needs to be done by playing with the concentration of exogenous biotin supplemented and tissue processed to enrich for biotintylated proteins to be detected by MS. Moving ahead proximity labelling seems like a promising tool to uncover novel meiotic genes regulating crossover designation supported by pilot experiments in this study highlighting its proof of principle. Interestingly, on examining the complementation of the transgenic lines generated for proximity labelling, we stumbled upon two intersting constructs namely HEI10-TbID and REC8-TbID. In case of REC8-TbID we observe that upon C-terminal tagging of REC8, there is premature depletion of the pericentromeric REC8 pool resulting in unbalanced segregation. Moving ahead this construct will be a valuable tool to study centromere proximal crossing over and role of REC8 in monopolar orientation. In case of HEI10-TbID we observed that C-terminal tagging of HEI10 allows it to load along the synaptonemal complex. However HEI10-TbID fails to coarsen and form large foci indicating that the intrinscially disordered C-terminal tail of HEI10 is important for its coarsening dynamics (Mercier et al, unpublished). Coupling this piece of evidence with another observation of this study namely HEI10 might possibly exist as a tetramer, the following model emerges, where HEI10 might exist as an oligomer driven by interactions of its N-terminal domain and the exposed residues of the intrinscially disordered C-terminal tail might plausibly govern its coaresning dynamics (Figure 26). However this needs further replicates to comment anything with statistical significance and validation at the cytological level to assess meiotic progression. Future experiments need to be directed to confirm this genetic data biochemically by approaches such as heterologous protein expression of HEI10 followed by size exclusion chromatorgraphy to confirm its oligomeric state.

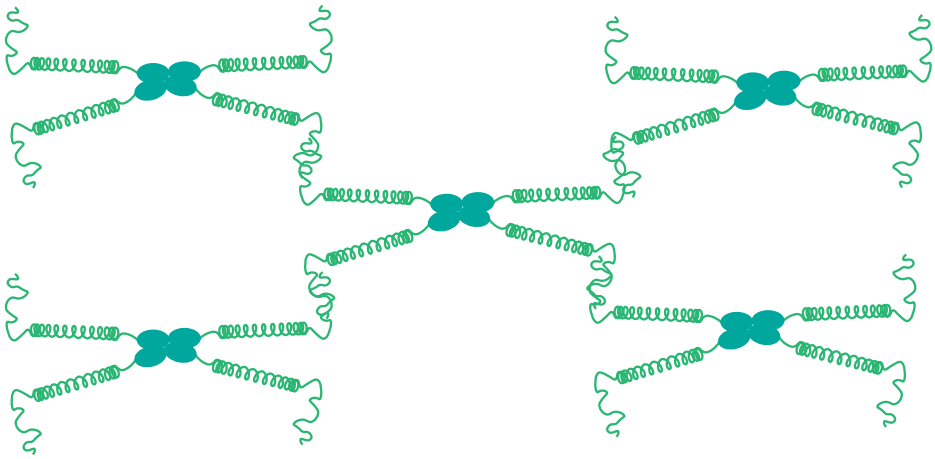

Figure 26| Model for multivalent interactions of HEI10 governing its coarsening dynamics
Each HEI10 monomer is believed to exist as a tetramer with its intrinsically disordered C-terminal tail facing outwards which might plausibly serve as a handle governing higher order interactions of HEI10 (Courtesy Hernán Lopez)

This study has also generated an extensive CRISPR-Cas9 collection of HEI10 mutants. Further analysis of these mutants undoubtedly will refine our understanding of the role played by different domains of HEI10 governing its coarsening dynamics. Studies of how chromosomes behave during meiosis in plants have so far almost exclusively relied on traditional microscopy techniques that kill the cells in the process of preparing them for imaging. While these techniques have been, and continue to be, very informative, they capture the underlying cellular dynamics only to a small degree. Importantly, these methods do not allow individual cells to be followed over time. Thus, conclusions about the course of meiocyte development and progression have to be deduced from the analysis of different cell populations at different time points. Live-cell imaging is a powerful method to obtain insights into cellular processes, particularly with respect to their dynamics. This is especially true for meiosis, where chromosomes and other cellular components such as the cytoskeleton follow an elaborate choreography over a relatively short period of time. Making these dynamics visible will expand our understanding of the regulation of meiosis. Recent advances in live-cell imaging in form of the Airyscan Laser Scanning confocal microscope [99] and development of bright and photostable fluorophores[100, 101], now equip us to analyse the meiotic events in plants in real time. These new microscopy methods rely on the generation of reporter lines for meiotic regulators and on the establishment of ex vivo culture and imaging conditions, which stabilize the specimen and keep it alive for several hours or even days[102, 103]. During the course of this thesis efforts were also made to develop fluorescently tagged lines of different meiotic genes which will soon make it possible to follow the enigmatic process of crossover designation in real type leveraging live cell imaging meiocytes.

Appendix

TAIR ID	Gene Name	Gene Description	A Module	B Module	C Module	D Module	E Module	F Module	Plant transformation Vector
AT1G67370	*ASY1*	HORMA DOMAIN protein forming lateral element of SC	ASY1 Promoter ~1.7 Kb	B-dummy	ASY1 CDS ~4.3 Kb	mStayGold(J) mScarlet-I3	ASY1 Terminator ~1.2 Kb	FastRed fluorescent selection	1. ASY1-mStaygold(J) 2. ASY-mScarletI3
AT1G33500	*SCEP1*	Coiled-coil protein forming central axis of SC	SCEP1 Promoter ~1.4 Kb	mStayGold(J) mScarlet-I3	SCEP1 CDS ~1.9 Kb	D-dummy	SCEP1 Terminator ~1.2 Kb	FastRed fluorescent selection	3. mStaygold(J)-SCEP1 4. mScarletI3-SCEP1
AT3G28370	*SCEP2*	Coiled-coil protein forming central axis of SC	SCEP2 Promoter ~2.2 Kb	mStayGold(J) mScarlet-I3	SCEP2 CDS ~3.1 Kb	D-dummy	SCEP2 Terminator ~2.3 Kb	FastRed fluorescent selection	5. mStaygold(J)-SCEP2 6. mScarletI3-SCEP2
AT4G26020	*SCEP3*	Central element of SC	SCEP3 Promoter ~1.5 Kb	mStayGold(J) mScarlet-I3	SCEP3 CDS ~1.9 Kb	D-dummy	SCEP3 Terminator ~2.3 Kb	FastRed fluorescent selection	7. mStaygold(J)-SCEP3 8. mScarletI3-SCEP3
AT1G12790	*PTD*	XPF-ERCC1 like endonuclease partnering with SHOC1	PTD Promoter ~2.5 Kb	B-dummy	PTD CDS ~1.6 Kb	mStayGold(J) mScarlet-I3	PTD Terminator ~1.7 Kb	FastRed fluorescent selection	9. PTD-mStaygold(J) 10. PTD-mScarletI3
AT5G48390	*ZIP4*	Tetra-tricopeptide repeat (TPR) protein facilitating protein -protein interactions	ZIP4 Promoter ~1.5 Kb	B-dummy	ZIP4 CDS ~3.3 Kb	mStayGold(J) mScarlet-I3	ZIP4 Terminator ~1 Kb	FastRed fluorescent selection	11. ZIP4-mStaygold(J) 12. ZIP4-mScarletI3
AT4G09140	*MLH1*	Mut1 DNA mismatch repair protein part of MutL complex required for dHJ resolution	MLH1 Promoter ~3.3 Kb	MLH1 Fragment 1 ~3.5 Kb	mStayGold(J) mScarlet-I3 TurboID	MLH1 Fragment 2 ~0.5 Kb	MLH1 Terminator ~1.2 Kb	FastRed fluorescent selection	13. MLH1 – mStaygold(J) $_{internal}$ 14. MLH1 – mScarletI3 $_{internal}$ 15. MLH1-TbID$_{internal}$

Table 6| List of fluorescent reporter lines generated (in process) for live cell imaging of meiosis. The plant transformation vectors were assembled using Greengate cloning [82] tagged with the fluorescent proteins mStaygold(J) and mScarlet-I3.

References

1. Mercier R., Mézard C., Jenczewski E., Macaisne N., Grelon M. 2015. The Molecular Biology of Meiosis in Plants. Annual Review of Plant Biology. **66**, 297–327.

2. Hofstatter P.G., Lahr D.J.G. 2019. All Eukaryotes Are Sexual, unless Proven Otherwise. BioEssays. **41**, 1800246.

3. Ramesh M.A., Malik S.-B., Logsdon J.M. 2005. A Phylogenomic Inventory of Meiotic Genes. Current Biology. **15**, 185–91.

4. Golubovskaya I.N. 1979. Genetic Control of Meiosis. In: International Review of Cytology., vol. 58. Elsevier, pp. 247–90.

5. Kaul M.L.H., Murthy T.G.K. 1985. Mutant genes affecting higher plant meiosis. Theoret. Appl. Genetics. **70**, 449–66.

6. Dawe R.K., Sedat J.W., Agard D.A., Cande W.Z. 1994. Meiotic chromosome pairing in maize is associated with a novel chromatin organization. Cell. **76**, 901–12.

7. Holá D. 1997. Neuffer, M.G., Coe, E.H., Wessler, S.R.: Mutants of Maize. Biologia plant. **39**.

8. Dawe R.K. 1998. MEIOTIC CHROMOSOME ORGANIZATION AND SEGREGATION IN PLANTS. Annu. Rev. Plant. Physiol. Plant. Mol. Biol. **49**, 371–95.

9. Zickler D., Kleckner N. 1998. THE LEPTOTENE-ZYGOTENE TRANSITION OF MEIOSIS. Annu. Rev. Genet. **32**, 619–97.

10. Zickler D., Kleckner N. 1999. Meiotic Chromosomes: Integrating Structure and Function. Annu. Rev. Genet. **33**, 603–754.

11. Hamant O., Ma H., Cande W.Z. 2006. GENETICS OF MEIOTIC PROPHASE I IN PLANTS. Annu. Rev. Plant Biol. **57**, 267–302.

12. Ma H. 2006. A Molecular Portrait of Arabidopsis Meiosis. The Arabidopsis Book / American Society of Plant Biologists. **4**.

13. Smyth D.R., Bowman J.L., Meyerowitz E.M. 1990. Early flower development in Arabidopsis. Plant Cell. **2**, 755–67.

14. Prusicki M.A., Balboni M., Sofroni K., Hamamura Y., Schnittger A. 2021. Caught in the Act: Live-Cell Imaging of Plant Meiosis. Front. Plant Sci. **12**, 718346.

15. Andersen S.L., Sekelsky J. 2010. Meiotic versus mitotic recombination: two different routes for double-strand break repair: the different functions of meiotic versus mitotic DSB repair are reflected in different pathway usage and different outcomes. Bioessays. **32**, 1058–66.

16. Huselid E., Bunting S.F. 2020. The Regulation of Homologous Recombination by Helicases. Genes (Basel). **11**, 498.

17. Gerton J.L., Hawley R.S. 2005. Homologous chromosome interactions in meiosis: diversity amidst conservation. Nat Rev Genet. **6**, 477–87.

18. Keeney S., Giroux C.N., Kleckner N. 1997. Meiosis-specific DNA double-strand breaks are catalyzed by Spo11, a member of a widely conserved protein family. Cell. **88**, 375–84.

19. Milman N., Higuchi E., Smith G.R. 2009. Meiotic DNA Double-Strand Break Repair Requires Two Nucleases, MRN and Ctp1, To Produce a Single Size Class of Rec12 (Spo11)-Oligonucleotide Complexes. Mol Cell Biol. **29**, 5998–6005.

20. Borde V., De Massy B. 2013. Programmed induction of DNA double strand breaks during meiosis: setting up communication between DNA and the chromosome structure. Current Opinion in Genetics & Development. **23**, 147–55.

21. Neale M.J., Pan J., Keeney S. 2005. Endonucleolytic processing of covalent protein-linked DNA double-strand breaks. Nature. **436**, 1053–7.

22. Harrison J.C., Haber J.E. 2006. Surviving the breakup: the DNA damage checkpoint. Annu Rev Genet. **40**, 209–35.

23. Lovejoy C.A., Cortez D. 2009. Common mechanisms of PIKK regulation. DNA Repair (Amst). **8**, 1004–8.

24. Caestecker K.W., Van de Walle G.R. 2013. The role of BRCA1 in DNA double-strand repair: Past and present. Experimental Cell Research. **319**, 575–87.

25. Scully R., Chen J., Plug A., Xiao Y., Weaver D., Feunteun J., Ashley T., Livingston D.M. 1997. Association of BRCA1 with Rad51 in mitotic and meiotic cells. Cell. **88**, 265–75.

26. Lord C.J., Ashworth A. 2007. RAD51, BRCA2 and DNA repair: a partial resolution. Nat Struct Mol Biol. **14**, 461–2.

27. Neale M.J., Keeney S. 2006. Clarifying the mechanics of DNA strand exchange in meiotic recombination. Nature. **442**, 153–8.

28. Kim K.P., Weiner B.M., Zhang L., Jordan A., Dekker J., Kleckner N. 2010. Sister Cohesion and Structural Axis Components Mediate Homolog Bias of Meiotic Recombination. Cell. **143**, 924–37.

29. Wang Y., Copenhaver G.P. 2018. Meiotic Recombination: Mixing It Up in Plants. Annual Review of Plant Biology. **69**, 577–609.

30. Börner G.V., Kleckner N., Hunter N. 2004. Crossover/noncrossover differentiation, synaptonemal complex formation, and regulatory surveillance at the leptotene/zygotene transition of meiosis. Cell. **117**, 29–45.

31. Snowden T., Acharya S., Butz C., Berardini M., Fishel R. 2004. hMSH4-hMSH5 recognizes Holliday Junctions and forms a meiosis-specific sliding clamp that embraces homologous chromosomes. Mol Cell. **15**, 437–51.

32. Pyatnitskaya A., Borde V., De Muyt A. 2019. Crossing and zipping: molecular duties of the ZMM proteins in meiosis. Chromosoma. **128**, 181–98.

33. Chelysheva L., Grandont L., Vrielynck N., le Guin S., Mercier R., Grelon M. 2010. An easy protocol for studying chromatin and recombination protein dynamics during

Arabidopsis thaliana meiosis: immunodetection of cohesins, histones and MLH1. Cytogenet Genome Res. **129**, 143–53.

34. Chelysheva L. et al. 2012. The Arabidopsis HEI10 Is a New ZMM Protein Related to Zip3. PLOS Genetics. **8**, e1002799.

35. Schwartz E.K., Heyer W.-D. 2011. Processing of joint molecule intermediates by structure-selective endonucleases during homologous recombination in eukaryotes. Chromosoma. **120**, 109–27.

36. Crismani W., Girard C., Froger N., Pradillo M., Santos J.L., Chelysheva L., Copenhaver G.P., Horlow C., Mercier R. 2012. FANCM Limits Meiotic Crossovers. Science. **336**, 1588–90.

37. Séguéla-Arnaud M. et al. 2015. Multiple mechanisms limit meiotic crossovers: TOP3α and two BLM homologs antagonize crossovers in parallel to FANCM. Proceedings of the National Academy of Sciences. **112**, 4713–8.

38. Ziolkowski P.A. 2023. Why do plants need the ZMM crossover pathway? A snapshot of meiotic recombination from the perspective of interhomolog polymorphism. Plant Reprod. **36**, 43–54.

39. Auxier B. et al. 2023. The human fungal pathogen Aspergillus fumigatus can produce the highest known number of meiotic crossovers. PLOS Biology. **21**, e3002278.

40. Wang S., Zickler D., Kleckner N., Zhang L. 2015. Meiotic crossover patterns: Obligatory crossover, interference and homeostasis in a single process. Cell Cycle. **14**, 305–14.

41. Fernandes J.B. et al. 2018. FIGL1 and its novel partner FLIP form a conserved complex that regulates homologous recombination. PLOS Genetics. **14**, e1007317.

42. Charlesworth D., Wright S.I. 2001. Breeding systems and genome evolution. Current Opinion in Genetics & Development. **11**, 685–90.

43. Durand S., Lian Q., Jing J., Ernst M., Grelon M., Zwicker D., Mercier R. 2022. Joint control of meiotic crossover patterning by the synaptonemal complex and HEI10 dosage. Nat Commun. **13**, 5999.

44. Láscarez-Lagunas L., Martinez-Garcia M., Colaiácovo M. 2020. SnapShot: Meiosis – Prophase I. Cell. **181**, 1442-1442.e1.

45. Wang M., Wang K., Tang D., Wei C., Li M., Shen Y., Chi Z., Gu M., Cheng Z. 2010. The Central Element Protein ZEP1 of the Synaptonemal Complex Regulates the Number of Crossovers during Meiosis in Rice. The Plant Cell. **22**, 417–30.

46. Capilla-Pérez L., Durand S., Hurel A., Lian Q., Chambon A., Taochy C., Solier V., Grelon M., Mercier R. 2021. The synaptonemal complex imposes crossover interference and heterochiasmy in Arabidopsis. Proceedings of the National Academy of Sciences. **118**, e2023613118.

47. France M.G., Enderle J., Röhrig S., Puchta H., Franklin F.C.H., Higgins J.D. 2021. ZYP1 is required for obligate cross-over formation and cross-over interference in Arabidopsis. Proc Natl Acad Sci U S A. **118**, e2021671118.

48. Ziolkowski P.A. et al. 2017. Natural variation and dosage of the HEI10 meiotic E3 ligase control Arabidopsis crossover recombination. Genes Dev. **31**, 306–17.

49. Morgan C., Fozard J.A., Hartley M., Henderson I.R., Bomblies K., Howard M. 2021. Diffusion-mediated HEI10 coarsening can explain meiotic crossover positioning in Arabidopsis. Nat Commun. **12**, 4674.

50. Kim J. et al. 2022. Arabidopsis HEAT SHOCK FACTOR BINDING PROTEIN is required to limit meiotic crossovers and HEI10 transcription. The EMBO Journal. **41**, e109958.

51. Nageswaran D.C. et al. 2021. HIGH CROSSOVER RATE1 encodes PROTEIN PHOSPHATASE X1 and restricts meiotic crossovers in Arabidopsis. Nat. Plants. **7**, 452–67.

52. Li Y., Qin B., Shen Y., Zhang F., Liu C., You H., Du G., Tang D., Cheng Z. 2018. HEIP1 regulates crossover formation during meiosis in rice. Proceedings of the National Academy of Sciences. **115**, 10810–5.

53. Singh D.K. et al. 2023. HEIP1 is required for efficient meiotic crossover implementation and is conserved from plants to humans. Proceedings of the National Academy of Sciences. **120**, e2221746120.

54. Dong C., Whitford R., Langridge P. 2002. A DNA mismatch repair gene links to the Ph2 locus in wheat. Genome. **45**, 116–24.

55. Emmanuel E., Yehuda E., Melamed-Bessudo C., Avivi-Ragolsky N., Levy A.A. 2006. The role of AtMSH2 in homologous recombination in Arabidopsis thaliana. EMBO reports. **7**, 100–5.

56. Ziolkowski P.A. et al. 2015. Juxtaposition of heterozygous and homozygous regions causes reciprocal crossover remodelling via interference during Arabidopsis meiosis. Ed D. Weigel. eLife. **4**, e03708.

57. Blackwell A.R. et al. 2020. MSH2 shapes the meiotic crossover landscape in relation to interhomolog polymorphism in Arabidopsis. The EMBO Journal. **39**, e104858.

58. Serra H., Svačina R., Baumann U., Whitford R., Sutton T., Bartoš J., Sourdille P. 2021. Ph2 encodes the mismatch repair protein MSH7-3D that inhibits wheat homoeologous recombination. Nat Commun. **12**, 803.

59. Girard C., Crismani W., Froger N., Mazel J., Lemhemdi A., Horlow C., Mercier R. 2014. FANCM-associated proteins MHF1 and MHF2, but not the other Fanconi anemia factors, limit meiotic crossovers. Nucleic Acids Research. **42**, 9087–95.

60. Kumar R., Duhamel M., Coutant E., Ben-Nahia E., Mercier R. 2019. Antagonism between BRCA2 and FIGL1 regulates homologous recombination. Nucleic Acids Res. **47**, 5170–80.

61. Knoll A., Higgins J.D., Seeliger K., Reha S.J., Dangel N.J., Bauknecht M., Schröpfer S., Franklin F.C.H., Puchta H. 2012. The Fanconi Anemia Ortholog FANCM Ensures Ordered Homologous Recombination in Both Somatic and Meiotic Cells in Arabidopsis. The Plant Cell. **24**, 1448–64.

62. Mieulet D. et al. 2018. Unleashing meiotic crossovers in crops. Nature Plants. **4**, 1010–6.

63. Chen H., He C., Wang C., Wang X., Ruan F., Yan J., Yin P., Wang Y., Yan S. 2021. RAD51 supports DMC1 by inhibiting the SMC5/6 complex during meiosis. The Plant Cell. **33**, 2869–82.

64. Zhu L. et al. 2021. Natural variation identifies SNI1, the SMC5/6 component, as a modifier of meiotic crossover in Arabidopsis. Proceedings of the National Academy of Sciences. **118**, e2021970118.

65. Sturtevant A.H. 1915. The behavior of the chromosomes as studied through linkage. Z.Ver-erbungslehre. **13**, 234–87.

66. Darlington C.D., Dark S.O.S. 1932. The Origin and Behaviour of Chiasmata, II. Cytologia. **3**, 169–85.

67. Rockmill B., Voelkel-Meiman K., Roeder G.S. 2006. Centromere-Proximal Crossovers Are Associated With Precocious Separation of Sister Chromatids During Meiosis in Saccharomyces cerevisiae. Genetics. **174**, 1745–54.

68. Sturtevant A.H. 1913. The linear arrangement of six sex-linked factors in Drosophila, as shown by their mode of association. J. Exp. Zool. **14**, 43–59.

69. Emerson S., Beadle G.W. 1933. Crossing-over near the spindle fiber in attached-X chromosomes ofDrosophila melanogaster. Z.Ver-erbungslehre. **65**, 129–40.

70. Mortimer R.K., Fogel S. 1974. Genetical Interference and Gene Conversion. In: Mechanisms in Recombination. Ed R.F. Grell. Boston, MA: Springer US, pp. 263–75.

71. Munz P. 1994. An analysis of interference in the fission yeast Schizosaccharomyces pombe. Genetics. **137**, 701–7.

72. Perkins D.D. 1962. CROSSING-OVER AND INTERFERENCE IN A MULTIPLY MARKED CHROMOSOME ARM OF NEUROSPORA. Genetics. **47**, 1253–74.

73. Chakraborty P., Pankajam A.V., Lin G., Dutta A., Krishnaprasad G.N., Tekkedil M.M., Shinohara A., Steinmetz L.M., Nishant K.T. 2017. Modulating Crossover Frequency and Interference for Obligate Crossovers in Saccharomyces cerevisiae Meiosis. G3 Genes|Genomes|Genetics. **7**, 1511–24.

74. Broman K.W., Weber J.L. 2000. Characterization of Human Crossover Interference. The American Journal of Human Genetics. **66**, 1911–26.

75. Zhang L., Wang S., Yin S., Hong S., Kim K.P., Kleckner N. 2014. Topoisomerase II mediates meiotic crossover interference. Nature. **511**, 551–6.

76. Zickler D., Kleckner N. 2016. A few of our favorite things: Pairing, the bouquet, crossover interference and evolution of meiosis. Seminars in Cell & Developmental Biology. **54**, 135–48.

77. Kleckner N., Zickler D., Jones G.H., Dekker J., Padmore R., Henle J., Hutchinson J. 2004. A mechanical basis for chromosome function. Proceedings of the National Academy of Sciences. **101**, 12592–7.

78. Girard C., Zwicker D., Mercier R. 2023. The regulation of meiotic crossover distribution: a coarse solution to a century-old mystery? Biochemical Society Transactions. **51**, 1179–90.

79. Zhang X., Henriques R., Lin S.-S., Niu Q.-W., Chua N.-H. 2006. Agrobacterium-mediated transformation of Arabidopsis thaliana using the floral dip method. Nat Protoc. **1**, 641–6.

80. Grützner R., Martin P., Horn C., Mortensen S., Cram E.J., Lee-Parsons C.W.T., Stuttmann J., Marillonnet S. 2021. High-efficiency genome editing in plants mediated by a Cas9 gene containing multiple introns. Plant Communications. **2**, 100135.

81. Engler C., Kandzia R., Marillonnet S. 2008. A One Pot, One Step, Precision Cloning Method with High Throughput Capability. PLOS ONE. **3**, e3647.

82. Lampropoulos A., Sutikovic Z., Wenzl C., Maegele I., Lohmann J.U., Forner J. 2013. GreenGate - A Novel, Versatile, and Efficient Cloning System for Plant Transgenesis. PLOS ONE. **8**, e83043.

83. L C. et al. 2019. Patronus is the elusive plant securin, preventing chromosome separation by antagonizing separase. Proceedings of the National Academy of Sciences of the United States of America. **116**.

84. Alexander M.P. 1969. Differential Staining of Aborted and Nonaborted Pollen. Stain Technology. **44**, 117–22.

85. Xu S.-L., Shrestha R., Karunadasa S.S., Xie P.-Q. 2023. Proximity Labeling in Plants. Annual Review of Plant Biology. **74**, 285–312.

86. Zhang L., Stauffer W., Zwicker D., Dernburg A.F. 2021. Crossover patterning through kinase-regulated condensation and coarsening of recombination nodules. 2021.08.26.457865.

87. Muyt A.D. et al. 2018. A meiotic XPF–ERCC1-like complex recognizes joint molecule recombination intermediates to promote crossover formation. Genes & Development. **32**, 283.

88. Arora K., Corbett K.D. 2019. The conserved XPF:ERCC1-like Zip2:Spo16 complex controls meiotic crossover formation through structure-specific DNA binding. Nucleic Acids Res. **47**, 2365–76.

89. Parisi S. et al. 1999. Rec8p, a Meiotic Recombination and Sister Chromatid Cohesion Phosphoprotein of the Rad21p Family Conserved from Fission Yeast to Humans. Molecular and Cellular Biology. **19**, 3515–28.

90. Yang C., Vizcay-Barrena G., Conner K., Wilson Z.A. 2007. MALE STERILITY1 Is Required for Tapetal Development and Pollen Wall Biosynthesis. Plant Cell. **19**, 3530–48.

91. Goldstein P. 1987. Multiple synaptonemal complexes (polycomplexes): origin, structure and function. Cell Biol Int Rep. **11**, 759–96.

92. Feng C. et al. 2023. TurboID-based proteomic profiling of meiotic chromosome axes in Arabidopsis thaliana. Nat. Plants. **9**, 616–30.

93. Zamariola L., De Storme N., Tiang CL., Armstrong S.J., Franklin F.C.H., Geelen D. 2013. SGO1 but not SGO2 is required for maintenance of centromere cohesion in Arabidopsis thaliana meiosis. Plant Reprod. **26**, 197–208.

94. Bhatt A.M., Lister C., Page T., Fransz P., Findlay K., Jones G.H., Dickinson H.G., Dean C. 1999. The DIF1 gene of Arabidopsis is required for meiotic chromosome segregation and belongs to the REC8/RAD21 cohesin gene family. The Plant Journal. **19**, 463–72.

95. Ronceret A., Gadea-Vacas J., Guilleminot J., Lincker F., Delorme V., Lahmy S., Pelletier G., Chabouté M.-E., Devic M. 2008. The first zygotic division in Arabidopsis requires de novo transcription of thymidylate kinase. Plant J. **53**, 776–89.

96. Deshaies R.J., Joazeiro C.A.P. 2009. RING Domain E3 Ubiquitin Ligases. Annual Review of Biochemistry. **78**, 399–434.

97. De Muyt A., Zhang L., Piolot T., Kleckner N., Espagne E., Zickler D. 2014. E3 ligase Hei10: a multifaceted structure-based signaling molecule with roles within and beyond meiosis. Genes Dev. **28**, 1111–23.

98. Rog O., Köhler S., Dernburg A.F. 2017. The synaptonemal complex has liquid crystalline properties and spatially regulates meiotic recombination factors. eLife. **6**, e21455.

99. Huff J. 2015. The Airyscan detector from ZEISS: confocal imaging with improved signal-to-noise ratio and super-resolution. Nat Methods. **12**, i–ii.

100. Gadella T.W.J., van Weeren L., Stouthamer J., Hink M.A., Wolters A.H.G., Giepmans B.N.G., Aumonier S., Dupuy J., Royant A. 2023. mScarlet3: a brilliant and fast-maturing red fluorescent protein. Nat Methods. **20**, 541–5.

101. Shimozono S., Ando R., Sugiyama M., Hirano M., Niino Y., Miyawaki A. 2024. Comparison of monomeric variants of StayGold. 2024.02.28.582207.

102. Prusicki M.A., Keizer E.M., van Rosmalen R.P., Komaki S., Seifert F., Müller K., Wijnker E., Fleck C., Schnittger A. 2019. Live cell imaging of meiosis in Arabidopsis thaliana. Eds C.S. Hardtke, D.C. Bergmann, J. Feijó. eLife. **8**, e42834.

103. Prusicki M.A., Balboni M., Sofroni K., Hamamura Y., Schnittger A. 2021. Caught in the Act: Live-Cell Imaging of Plant Meiosis. Frontiers in Plant Science. **12**.